D1-mGlu5 heteromers mediate noncanonical dopamine signaling in Parkinson's disease

Irene Sebastianutto, Elise Goyet, Laura Andreoli, Joan Font-Ingles, David Moreno-Delgado, Nathalie Bouquier, Céline Jahannault-Talignani, Enora Moutin, Luisa Di Menna, Jean-Philippe Pin, et al.

D1 and mGlu5 heteromers mediate non-canonical dopamine signaling in Parkinson's disease.

Irene Sebastianutto[§1], Elise Goyet[§2], Laura Andreoli[+1], Joan Font-Ingles[+2], David Moreno-Delgado[+2,5], Nathalie Bouquier[2], Céline Jahannault-Talignani[2], Enora Moutin[2], Luisa Di Menna[3], Natallia Maslava[1], Jean-Philippe Pin[2], Laurent Fagni[2], Ferdinando Nicoletti[3,4], Fabrice Ango[2], M. Angela Cenci*[1], and Julie Perroy*[2]

[1] Basal ganglia pathophysiology unit, Dept. Experimental Medical Science, Lund University, Lund, Sweden.

[2] IGF, Univ. Montpellier, CNRS, INSERM, Montpellier, France.

[3] I.R.C.C.S. Neuromed, Pozzilli, Italy.

[4]Dept. Physiology and Pharmacology, Sapienza University of Rome, Italy.

[5] Department of Neuroscience Research, UCB Pharma, Braine l'Alleud, Belgium.

[§] Shared first authors

[+] Shared second authors

* Shared senior and corresponding authors
M. Angela Cenci, Angela.Cenci_Nilsson@med.lu.se
Julie Perroy, Julie.perroy@igf.cnrs.fr

Key words: movement disorders, dopamine replacement therapy, motor complications, basal ganglia, G-protein coupled receptor, oligomers, Fluorescence / Bioluminescence Resonance Energy Transfer.

Abstract

Dopamine receptor D1 modulates glutamatergic transmission in cortico-basal ganglia circuits and represents a major target of L-DOPA therapy in Parkinson's disease. Here we show that the D1 receptor and metabotropic glutamate receptor type 5 (mGlu5) can form previously unknown heteromeric entities with distinctive functional properties. Interacting with Gq proteins, cell surface D1-mGlu5 heteromers exacerbate phospholipase C (PLC) signaling and intracellular calcium release in response to either glutamate or dopamine. In rodent models of Parkinson's disease, D1-mGlu5 nanocomplexes are strongly up-regulated in the dopamine-denervated striatum, resulting in a synergistic activation of PLC signaling by D1 and mGlu5 receptor agonists. In turn, D1-mGlu5-dependent PLC signaling is causally linked with excessive activation of extracellular signal-regulated kinases in striatal neurons, leading to dyskinesia in animals treated with L-DOPA or D1 receptor agonists. The discovery of D1-mGlu5 functional heteromers mediating maladaptive molecular and motor responses in the dopamine-denervated striatum may prompt the development of novel therapeutic principles for Parkinson's Disease.

Introduction

Functional interactions between dopamine (DA) and glutamate (Glu) are critical to the functions of the striatum, where dopaminergic and glutamatergic signals are integrated to control movement vigor, action selection, habit formation, and reinforcement learning (1–3). In Parkinson's disease (PD), a severe degeneration of dopaminergic nigrostriatal projections leads to impairments in striatal synaptic plasticity and the associated motor and cognitive functions (4). Pharmacological DA replacement with L-DOPA may initially correct some of these impairments (5), but with the progression of PD this treatment causes dyskinesia (abnormal involuntary movements) in a majority of the patients. L-DOPA-induced dyskinesia (LID) depends on a dysfunctional interplay between DA and Glu signaling whose molecular basis is poorly understood. What is clear is that dopamine D1 receptors play a pivotal role in striatal signaling abnormalities and synaptic plasticity deficits associated with LID (6–8).

Metabotropic glutamate type 5 (mGlu5) receptors are coexpressed with D1 in about 50% of striatal neurons (9) and they are regarded as a potential therapeutic target for the treatment of LID (reviewed in (10). Indeed, pharmacological antagonism of mGlu5 improves peak-dose LID and counters an abnormal striatal activation of extracellular signal-regulated kinases 1 and 2 (ERK1/2) downstream of D1 receptors (11).

We set out to address the hypothesis that the formation of signaling platforms involving both D1 and mGlu5 proteins may lead to a dysfunctional cross-talk between these receptors in DA-denervated striatal neurons. Such a process could be favored by the relocalisation of a postsynaptic pool of D1 receptors following DA denervation (5). Using Bioluminescence resonance energy transfer (BRET) and Bimolecular Fluorescence Complementation, we here demonstrate for the first time that mGlu5 and D1 receptors do form heteromers at the plasma membrane both in a heterologous expression system and in neurons. Interestingly, D1-mGlu5 receptor heteromers are Gq-coupled and mediate a synergistic activation of PLC signaling and intracellular Ca^{2+} release by the respective receptor agonists. By applying a proximity ligation assay to striatal tissue from adult rodents, we show that D1-mGlu5 complexes increase in abundance after DA denervation and persist in face of DA replacement therapy. Accordingly, DA-denervated striata exhibit a synergistic potentiation of PLC signaling upon treatment with D1 and mGlu5 agonists. Finally, we provide evidence that a D1- and mGlu-dependent PLC activation is causally linked with both striatal ERK1/2

signaling and dyskinetic behaviours in rodent models of PD. Taken together, these data indicate that an increased abundance of D1-mGlu5 heteromers is a molecular trait of DA-denervated striatal neurons and that it is causal to a maladaptive signaling response to DA replacement therapy.

Results

D1 and mGlu5 receptors form heteromers in vitro.

When co-expressed in HEK cells, D1 and mGlu5 receptors co-localized at the cell surface (suppl. Figure S1A). To assess a possible direct physical interaction between D1 and mGlu5 receptors, we performed BRET assays in this cell population. The energy donor Renilla luciferase 8 (Rluc8) was fused to the N-terminus of mGlu5 and the acceptor yellow fluorescent protein Venus to the N-terminus of D1 receptor (Rluc8-mGlu5 and Venus-D1, respectively). At constant level of Rluc8-mGlu5 expression, the BRET signal increased hyperbolically as a function of the Venus-D1 acceptor expression level (fluorescence/luminescence ratio) (Figure 1A). Saturation of the BRET signal when all Rluc8-mGlu5 was bound to Venus-D1 reported a specific interaction between the mGlu5 and D1 receptors in living cells. As non-radiative energy transfer requires close proximity (< 75 Å) between the acceptor and the donor (12), these BRET experiments demonstrate that mGlu5 and D1 receptors are close enough to form heteromers. This saturable interaction was further confirmed measuring the BRET signal between full-length mGlu5 and D1 receptors tagged in C-terminal position with Nano luciferase (Nluc) and Venus (mGlu5-Nluc and D1-Venus, respectively, Figure 1B). The C-terminal tails of mGlu5 and D1 receptors have been reported to mediate interactions with other G-protein coupled receptors (GPCRs), such as the □ opioid one (13), or with NMDA receptors (14, 15). Deletion of mGlu5 C-tail did not alter correct expression of the receptor at the cell surface (Rluc8-mGlu5DelCT, Suppl. Figure S1B), but prevented its interaction with D1 (Figure 1A). Now the BRET signal between Rluc8-mGlu5DelCT and Venus-D1 receptors increased linearly with the latter's expression levels (Figure 1A, black curve), most likely reflecting random collision between mGlu5DelCT and D1 receptors. Consistently, co-expression of a plasma membrane-targeted mGlu5 C-tail (CD4-CtailmGlu5) as a dominant negative peptide decreased the BRET signal (Figure 1C), confirming the involvement of mGlu5 C-tail in the receptor interaction. Using the same methodology, we further tested other D1 and mGlu5 potential partners. For a constant

expression of D1-Rluc receptor, the BRET signal increased hyperbolically as a function of mGlu1-YFP expression level (Figure S2A), reporting a specific interaction between D1 and mGlu1 receptors, which are quite similar to mGlu5 regarding molecular structure and signal transduction properties (16). Using the same method, mGlu5 was found able form heteromers with the D2 receptor (Fig. S4B). By opposition, we found no specific BRET signal between D1 and β2 adrenergic receptors, nor between mGlu5 and GABAb receptors (see the linear increase in BRET signal, Suppl. Figure S2 C,D), despite previous demonstrations of functional signaling interactions between these receptor categories in different neuronal systems (17–20). These data indicate that the heteromerization process is not random, receptors can only associate with specific partners.

We further assessed the cellular localization of the D1-mGlu5 heteromer by Bimolecular Fluorescence Complementation (BiFC) assays, a protein fragment complementation method appropriate to visualize GPCR oligomerization (21, 22) (Figure 1D). We fused complementary Venus1 (V1) and Venus2 (V2) fragments to the C-termini of D1 and mGlu5 receptors (D1-V1, D1-V2, mGlu5-V1 and mGlu5-V2, respectively, Figure 1E). As expected from BRET results, co-expression of D1-V1 and mGlu5-V2 in HEK cells resulted in the reconstitution of a fluorescent Venus protein, confirming the ability of these receptors to form heteromers (Figure 1E). Co-localization of Venus-fluorescence intensity with a red fluorescent plasma membrane protein (pmRFP) further highlighted a preferential expression of D1-V1/mGlu5-V2 heteromers at the cell surface (65.66 ± 12.57 % of total Venus fluorescence co-localized with pmRFP, Figure 1F). This cell surface preferential expression of the heteromer was significantly lower than D1-V1/D1-V2 (73.35 ± 12.46 %) and higher than mGlu5-V1/mGlu5-V2 homodimers (60.04 ± 12.62%, Figure 1F). Altogether, these data disclose the existence of D1-mGlu5 heteromers, preferentially localized at the cell surface of HEK cells.

D1 and mGlu5 receptors also formed heteromers in primary, cultured hippocampal neurons (Figure 2), which endogenously express these receptors (Suppl. Figure S1C) (23, 24). The BRET signal between mGlu5-Nluc and D1-Venus in hippocampal neurons was indeed significantly higher than the basal BRET measured in cells expressing the BRET donor alone (Figure 2A-B). Because cultured hippocampal neurons form dendrites and spines, we were able to assess the relative localization of D1-mGlu5 heteromers in different cellular compartments, finding a higher BRET signal in dendritic shafts and spines compared to the cell soma (Figure 2A, see 535/480 ratio image in upper row, and quantification in Figure 2C, $p <$

0.05 for spines vs. soma). This subcellular pattern is reminiscent of the preferential distribution of native D1 and mGlu5 in spines and dendrites relative to perikaryal regions (25–27). We did not carry out this experiment in primary striatal cultures because the striatal neurons expressing both D1 and mGlu5 receptors (so-called medium spiny neurons) are aspiny in culture.

Functional properties of D1-mGlu5 heteromers.

We next interrogated the functional consequences of D1-mGlu5 receptor heteromerization. Using a time resolved (TR)-FRET based sensor, we measured extracellular conformational changes within mGlu5 receptor homodimer (Figure 3A). Upon receptor and G-protein activation, the reorientation of the extracellular ligand-binding domains (ECDs) of the mGlu5 homodimer subunits results in a decrease of the FRET signal (28). Interestingly, in absence of ligand, the proportion of mGlu5 receptors in active-like conformation increased hyperbolically as a function of the D1-Venus expression level ('No Ligand', Figure 3B). This result reveals a D1 receptor-induced basal activation of mGlu5 receptor that saturates (at around 30% of maximal mGlu5 activation rate) for high D1 receptor expression level. D1 receptor co-expression did not affect Emax nor EC_{50} of mGlu5 agonist (quisqualic acid) or antagonist (LY341495) (Figure 3B, C). This conformational change of mGlu5 was triggered by its physical interaction with D1. Impairment of D1-mGlu5 interaction by co-expression of mGlu5-Ctail fused to plasma membrane (CD4-Ctail, Figure 1B) significantly reduced the amount of mGlu5 receptors displaying an active conformation (Figure 3D), while receptors expression was not changed (Figure 3E). Consistently, mGlu5 sensor deleted from its C-tail (which cannot interact with D1, cf. Figure 1A) was not affected by D1 co-expression (Figure 3F). Hence, under basal conditions, D1-mGlu5 heteromerization favors an active conformation of mGlu5.

We next studied the functional consequences of D1-induced enhancement of mGlu5 receptors in active conformation. Since mGlu5 canonical coupling to Gq induces PLC pathway activation, we assessed phosphoinositide (PI) hydrolysis by measuring the production of inositolmonophosphate (InsP), originated from the sequential dephosphorylation of inositol-1,4,5-trisphosphate (Figure 3G). For a constant expression of mGlu5 receptors, basal InsP levels increased hyperbolically as a function of the D1-Venus expression levels to reach 30% of the maximal agonist-induced InsP production (Figure 3H). Moreover, the slope of constitutive

InsP production induced by increasing expression level of mGlu5 was higher in the presence than in the absence of D1 receptor (Figure 3I). Hence, D1-mGlu5 heteromerization not only enhanced the rate of mGlu5 receptors in active-like conformation, but also the basal InsP production.

To further analyze the functional consequences of mGlu5 and D1 co-expression on their respective canonical signaling pathways (Gq and Gs-preferential coupling, respectively), we generated a HEK cell-line stably expressing two sensors, the GCaMP6 fluorescent calcium sensor and the Glo luminescent cAMP sensor (Figure 4A). While D1-like agonist (SKF81297) induced cAMP production but not Ca^{2+} release on cells expressing D1 alone (red traces, Figure 4D and B, respectively), the co-expression of mGlu5 enabled D1-like agonist-induced Ca^{2+} release (Figure 4B, purple trace) and did not affect the potency of SKF81297 to induce cAMP production (Figure 4D, purple trace). This result suggested that an allosteric interaction between mGlu5 and D1 receptors allows the D1 receptor to signal through a Ca^{2+} release pathway. On the other side, the mGlu5 agonist quisqualate induced a similar Ca^{2+} response in the presence or absence of co-expressed D1 receptors (Figure 4C, purple and blue traces). In agreement with recent reports (29), we noticed that the mGlu5 agonist induced cAMP production when mGlu5 was expressed alone, and this property was not affected by D1 co-expression (Figure 4E). The application of SKF81297 did not induce Ca^{2+} release in cells expressing only D1 receptors (Figure 4F) or mGlu5 receptors (Figure 4G). In contrast, when both receptors were coexpressed, the coapplication of a mGlu5 agonist (quisqualate 50 nM) and SKF81297 produced a 3-fold increase in Ca^{2+} release above baseline levels (Figure 4H). Taken together, these results suggest that the D1-mGlu5 heteromer has a signaling bias towards Ca^{2+}-dependent pathways and mediates a synergistic activation of such pathways upon stimulation.

The biased Ca^{2+} signaling associated with D1 and mGlu5 co-expression could be driven by activation of Gq type proteins by the heteromer. To specifically study Gq protein binding to the heterodimer, we used complemented donor-acceptor resonance energy transfer (CODA-RET) (30) combining BiFC and BRET (Figure 5A). We took profit of the BiFC combinations described in Figure 1D to follow exclusively one signaling at a time, coming from D1-V1/D1-V2, mGlu5-V1/mGlu5-V2 or D1-V1/mGlu5-V2 (Figure 5B). BRET imaging revealed an interaction of the D1-mGlu5 heteromer with the Nluc-G□q subunit of the G□q□1□2

heterotrimer (Figure 5C). Consistent with the canonical G-protein coupling described for those receptors, BRET imaging also showed a Gq interaction with mGlu5 homomers (Figure 5D) but not with D1 homomers (Figure 5E).

D1 and mGlu5 form abundant receptor complexes in the DA-denervated striatum

The biochemical properties of D1-mGlu5 heteromers are reminiscent of signaling features typical of DA-denervated striatal neurons, where D1 and mGlu5 functionally interact and activate extracellular signaling-regulated kinases 1 and 2 (ERK1/2) in a manner that requires PLC activity and Ca^{2+} release from intracellular stores (11). To search for D1-mGlu5 complexes in DA-denervated striatal neurons, we prepared mice with unilateral 6-hydroxydopamine (6-OHDA) lesions of the medial forebrain bundle (MFB) and then processed both intact and DA-denervated striatal tissue for Proximity Ligation Assay (PLA) with antibodies against D1 and mGlu5. With in situ PLA, fluorescent-labeled complementary oligonucleotide probes bind to the amplicons (amplified DNA) at the sites of protein-protein interaction, producing distinct dots of high fluorescence on the tissue. Fluorescence dots were clearly detectable although sparse in the intact striatum (Figure 6A-B), and their abundance increased by approximately 2.5-fold in DA-denervated samples (Figure 6C-D; $p < 0,05$ for lesioned vs intact striatum), indicating a higher association of mGlu5 with D1 receptors after nigrostriatal dopaminergic degeneration. The number of D1-mGlu5 puncta was further increased after a chronic dyskinesiogenic course of L-DOPA treatment (Figure 6E-F). Transgenic mice with a selective genetic ablation of mGlu5 in D1-expressing neurons (*mGluR5*$^{KO\text{-}D1}$) did not exhibit a distinct signal (Figure 6G-H), attesting the specificity of our PLA methodology.

D1-mGlu5 synergistically activate PLC signaling in the DA-denervated striatum.

mGlu5 is a Gq-coupled receptor and its stimulation leads to phosphoinositide hydrolysis via PLCβ (31). While stimulation of bona fide D1 receptors does not activate PLC, our data so far indicate that such a response would occur in the presence of D1-mGlu5 heteromers. To test this prediction, we used an ex vivo assay of PLC activity measuring the production of ^{3}H-InsP (32) and compared the effects of D1/mGlu5 stimulation in DA-denervated or intact striata.. For this assay, we used 6-OHDA-lesioned rats rather than mice because we needed a large amount of striatal tissue (see Methods). Striatal samples were incubated with the D1-like

agonist SKF38393, the mGlu1/5 receptor agonist DHPG, or their combination in the presence of mGlu1 blockade (achieved using saturating concentrations of JNJ16259685). When applied alone, both SKF38393 and DHPG tended to enhance ^{3}H-InsP levels in both intact and DA-denervated striata, but only the effect of SKF38393 in the lesioned striatum reached statistical significance (Figure 7A, SKF38393 vs. basal: 46% increase, $p < 0.05$). The coapplication of SKF38393 and DHPG produced a significant increase in ^{3}H-InsP production in both intact and denervated samples, but the effect of agonists coapplication was markedly larger in the presence of DA denervation (Figure 7A, 141% vs. 70% increase above basal levels in lesioned vs intact striatum, respectively; $p < 0.001$). This effect was blocked by coincubation with the mGlu5 antagonist MTEP (Figure 7A). In DA-denervated samples, the effect of SKF38393-DHPG coapplication was over two-fold larger than the sum of changes produced by each agonist alone, indicating a synergistic activation of PLC signaling (Figure 7A). These data suggest that a concomitant increase in DA and glutamate levels in the parkinsonian striatum would lead to a strong activation of PLC in cells expressing both D1 and mGlu5 receptors.

Because striatal levels of both DA and glutamate increase in PD shortly after the administration of L-DOPA (33, 34), we set out to examine the effects of PLC inhibition in unilaterally 6-OHDA-lesioned rats treated with L-DOPA using ERK1/2 activation as a molecular marker of aberrant D1-mGlu5 dependent signaling (11). Animals were perfusion-fixed 30 min following the combined administration of L-DOPA and the systemically active, selective PLC inhibitor U73122. As expected (36), L-DOPA (6 mg/kg s.c.) produced a large induction of the active, phosphorylated form of ERK1/2 in DA-denervated, but not intact striata (Figure 7C-D). Throughout the DA-denervated striatum, the effect of L-DOPA was substantially reduced in animals cotreated with U73122 (30 mg/kg i.p.; Figure 7C-D). The magnitude of such reduction was comparable to that produced by MTEP in a previous study (37). In other groups of 6-OHDA-lesioned rats, we examined the effects of the selective D1- and D2-like agonists SKF38393 and quinpirole, respectively. While quinpirole did not have any inducing effect on ERK1/2 (data not shown), the D1 agonist SKF38393 (2 mg/kg s.c.) produced robust ERK1/2 activation throughout the DA-denervated striatum, and also this response was substantially attenuated by U73122 (Figure 7E-F). Next, we verified the effect of PLC inhibition on D1-dependent ERK1/2 activation using both wild-type and *mGlu5*$^{KO\text{-}D1}$ mice. As expected (11), SKF38393 induced a large number of pERK1/2-positive cells in the DA-denervated striatum of wild-type mice, and a significantly lower number in *mGlu5*$^{KO\text{-}D1}$ *mice* (Figure 7 G-H). In wild-

type mice, the effect of SKF38393 was significantly blunted by U73122 cotreatment (Figure 7 G-H). In contrast, there was no difference between vehicle and U73122 coadministration in lesioned *mGluR5*$^{KO\text{-}D1}$ mice treated with SKF38393 (Figure 7G). These data indicate that the absence of mGlu5 receptor in D1-positive neurons occludes the molecular pathway through which U73122 attenuates the aberrant striatal activation of ERK1/2.

In summary, these data show that PLC signaling accounts for a significant proportion of striatal ERK1/2 activation in parkinsonian animals treated with drugs that stimulate the D1 receptor. The residual, PLC-independent ERK1/2 activation most likely reflects the supersensitivity of D1-mediated cAMP/PKA signaling after DA denervation, because this signaling response is not affected by the inhibition of either mGlu5 or PLC (11).

Inhibition of PLC or mGlu5 receptors reduces dyskinesias that depend on D1 receptors stimulation

Marked striatal activation of ERK1/2 by L-DOPA is a maladaptive molecular response causally linked with dyskinesia (35), and cotreatment with mGlu5 antagonists blunts both L-DOPA-induced ERK1/2 activation and L-DOPA-induced peak AIMs, that is, the most disabling dyskinesias appearing when brain levels of L-DOPA are high (38, 39). We therefore set out to examine potential antidyskinetic effects of PLC inhibition in parkinsonian rodents chronically treated with dopaminergic agents. Mice with unilateral 6-OHDA lesions in the MFB sustained three consecutive drug treatment periods using escalating doses of L-DOPA (3 and 6 mg/kg), SKF38393 (3 and 6 mg/kg), or quinpirole (0.1 and 0.5 mg/kg). With this protocol, the three different dopaminergic drugs induced similarly severe abnormal involuntary movements (AIMs) by the end of each treatment period, at which point we compared the effects of PLC inhibition with U73122 or selective mGlu5 antagonism with MTEP.

The peak severity of L-DOPA-induced AIMs was reduced by both U73122 and MTEP (Figure 8A, $p < 0.05$ for each compound versus vehicle at 20-80 min post L-DOPA administration) to a comparable extent (Figure 8B). Treatment with the D1-like agonist SKF38393 induced severe and sustained AIMs, which were significantly attenuated by U73122 and MTEP with a comparable temporal course (Figure 8C-D). The D2 receptor agonist quinpirole can induce dyskinesia in rodents primed with L-DOPA or D1 agonists (40). We exploited this phenomenon to investigate the efficacy of U73122 or MTEP on dyskinesias that are mediated via the D2 receptor. When mice were challenged with quinpirole, alone or

combined with U73122 or MTEP, neither the PLC inhibitor nor the mGlu5 receptor antagonist had any antidyskinetic action (Figure 8E-F). The pattern of antidyskinetic effects by PLC inhibition and mGlu5 antagonism was identical in the rat model of LID, in which we also verified that pharmacological inhibition of PLC did not interfere with the anti-akinetic (therapeutic-like) effect of the dopaminergic agents (see rat AIMs and motor test in Suppl. Figure S3). Moreover, using this model we showed that pharmacological inhibition of muscarinic receptors with dicyclomine (41) did not have any antidyskinetic effect (see Suppl. Figure S3J-K). This experiment rules out the possibility that the PLC activity contributing to LID is downstream of the Gq-coupled muscarinic receptor M1, which is abundantly expressed in striatal projection neurons (i.e., the cells expressing active ERK1/2 upon treatment with L-DOPA or SKF38393, (11, 36)).

We next set out to verify whether the antidyskinetic effects of U73122 or MTEP are mediated by neurons that coexpress both D1 and mGlu5 receptors. To this end, we applied the same protocol of 6-OHDA lesions and dopaminergic treatments to the *mGluR5*$^{KD\text{-}D1}$ conditional transgenic mouse, which displays an almost complete loss of mGlu5 in striatal neurons expressing the D1 receptor (9) and a blunted striatal ERK1/2 response to D1 stimulation in a parkinsonian setting (11). Transgenic *mGluR5*$^{KD\text{-}D1}$ mice responded to the 6-OHDA lesion in the same way as did wild-type mice (Suppl. Figure S4A-B), and they also showed a similar anti-akinetic response to L-DOPA in a test of forelimb use (Suppl. Figure S4C). However, compared to their wildtype littermates, transgenic *mGluR5*$^{KD\text{-}D1}$ mice developed significantly milder dyskinesias when treated with L-DOPA or SKF38393 (see Suppl. Figure S4D-E and F-G for a direct genotype comparison). When challenged with either U73122 or MTEP, *mGluR5*$^{KD\text{-}D1}$ mice showed no further reductions in peak AIM scores as induced by either L-DOPA (Figure 8G-H) or SKF38393 (Figure 8I-J), although the duration of SKF38393-induced dyskinesia appeared shorter after cotreatment with either compound (Figure 8I; $p < 0.05$ at 120 min for both U73122 and MTEP vs. vehicle cotreatment in the SKF38393 experiment). By contrast, quinpirole-induced AIMs were as severe in *mGluR5*$^{KD\text{-}D1}$ mice as in wildtype controls (cf. Figure 8E and K, and Suppl. Figure S4J-K) and remained completely unaffected by U73122 or MTEP cotreatment (Figure 8K-L).

Taken together, these results demonstrate that, in parkinsonian animals treated with dopaminergic agents, the same pattern of antidyskinetic effects is obtained by antagonizing

either mGlu5 or PLC signaling. These antidyskinetic effects occur downstream of D1 receptor stimulation and are mediated by neurons that coexpress D1 and mGlu5 receptors.

Discussion

In cognitive, limbic and motor brain networks, glutamatergic neurotransmission is under the pivotal control of dopaminergic afferents. The present work contributes to an improved understanding of the interplay between dopaminergic and glutamatergic signaling by revealing unheralded physical and functional interactions between D1 and mGlu5 receptors, two important therapeutic targets in several neuropsychiatric diseases (10, 42). Using recent improvements in single-cell BRET imaging (43), we demonstrate for the first time the occurrence of D1-mGlu5 heteromers displaying atypical properties compared to the homomers. D1-mGlu5 heteromers interact with Gq proteins and enable a synergistic activation of PLC signaling and intracellular calcium release by their respective agonists. The native receptors in the striatum can form nanocomplexes revealed as fluorescent dots by the PLA assay, a method used to report a theoretical maximum distance of 30 nm between two target proteins (44). These receptor complexes become abundant and functionally significant after a lesion of nigrostriatal dopaminergic projections mimicking PD. Accordingly, in the DA-denervated striatum, the co-stimulation of D1 and mGlu5 leads to a synergistic activation of PLC. Inhibiting PLC signaling counters maladaptive molecular and behavioral responses to L-DOPA, the most important form of DA replacement therapy in PD.

In addition to reporting a physical interaction between D1 and mGlu5 receptors, the present study reveals the peculiar functional properties of this new signaling complex. Thus, in HEK cells expressing D1-mGlu5 heteromers, D1-like agonists trigger both the expected increase in cAMP production and an atypical release of intracellular Ca^{2+}. Taken together, our cellular assays indicate that D1-mGlu5 heteromers can lead to a potentiation of PLC/Ca^{2+}-dependent signaling both by increasing mGlu5 constitutive activity and by biasing a pool of D1 receptors towards activating this pathway. Moreover, our results predict that D1-mGlu5 heteromers would mediate a synergistic activation of PLC/Ca^{2+}-dependent signaling in the presence of both receptor agonists.

The administration of L-DOPA results in a surge of striatal DA and glutamate levels in in both PD patients and animal models of PD (29, 30). These neurochemical changes concur to produce a strong striatal activation of ERK1/2 signaling, a master switch of synaptic, transcriptional and epigenetic changes that mediate dyskinetic behaviours (35, 45, 47–49). Despite that NMDA- and D1 receptors cooperate to activate ERK1/2 in the intact striatum (50,

51), NMDA receptor antagonists have no effect on the ERK1/2 response to L-DOPA in DA-denervated striatal neurons (11, 37). Instead, this maladaptive ERK1/2 response results from a functional interaction between D1 and mGlu5 receptors (11, 36). Using DA-denervated striatal slices incubated with SKF38393, we have previously shown that D1 agonist-induced ERK1/2 activation is both PLC- and Ca^{2+}-dependent (11). Taken together, these previous findings have suggested that the D1 receptor engages in a preferential cross-talk with mGlu5 and Gq-related signaling components in DA-denervated striatal neurons. The present study offers a plausible molecular explanation to such a phenomenon. Indeed, the results of our cellular assays reveal that D1-mGlu5 heteromers couple to Gq-type proteins and mediate a synergistic activation of PLC/$Ca2^{+}$ signaling by the respective agonists. Consistent with these results, an assay of InsP production in rodent models reveals synergistic activation of PLC signaling by D1 and mGlu5 agonists specifically in the DA-denervated striatum. Accordingly, the PLA data show that D1-mGlu5 receptor nanocomplexes become significantly more abundant in the striatum after DA denervation. Plausibly, the larger abundance of D1-mGlu5 receptor clusters in the DA-denervated striatum is linked to changes in D1 receptor localisation occurring after a loss of dopaminergic inputs. In particular, a relocalisation of D1 receptors away from synaptic membranes, as reported in DA-denervated rodents (5), would facilitate an association of D1 proteins with the mGlu5 receptor, which normally resides in perisynaptic membranes (25).

The heteromerization process increases the diversity of a receptor's signaling through functional platforms (52). However, possibilities of interaction are not random and their specificity seems tightly controlled. For example, we have previously shown two distinct groups of association compatibility between mGlu receptors subtypes (53): group I mGlu receptors (subtypes 1 and 5) interact together, but do not associate with others, while group II (subtypes 2 and 3) and III mGlu receptors (subtypes 4, 7, and 8) preferentially associate with each other but not with those from group I. Similarly, we showed that Group I mGlu1 receptors do not interact with GABAb receptors which are however co-expressed in Purkinje neurons and functionally coupled (54). In the scope of the present work, we further tested other D1 and mGlu5 potential partners. We report no specific BRET signal between D1 and β2 adrenergic receptors, nor between mGlu5 and GABAb receptors, suggesting that those pairs of GPCRs cannot form heteromers, despite their demonstrated capacity for cross-interaction in neural modulation (17–20). In these cases, converging signaling pathways downstream of

the receptors might be involved rather than a direct physical association. By opposition, we found specific BRET signals between D1 and mGlu1 receptors, which is a previously unknown interaction. Importantly, mGlu1 and mGlu5 receptors share a high degree of sequence homology and signal-transduction properties (16), but they differ substantially in terms of striatal expression levels (55). We furthermore found an interaction between mGlu5 and D2 receptors, which is in agreement with previous publications showing that D2, mGlu5, and A2a receptors can be found in the same complexes (56, 57). Beyond receptor structure, cellular context and physio/pathological conditions might be permissive or not to specific interactions. Related to the striatum, a pathogenic role of heteromers involving D1 receptors has already been reported. In particular, it has been proposed that physical interactions between D1 and NMDA GluN1 (58) or D1 and D3 receptors (59) play a causal role in LID. However, these previously described heteromers were unequivocally induced by the chronic treatment with L-DOPA, often leading to an upregulation of the involved receptor proteins. By contrast, we here report that the D1-mGlu5 assembly is prompted by DA denervation and further maintained upon chronic L-DOPA treatment. Therefore, our results uncover a novel molecular determinant of denervation-induced signaling abnormalities that potently predispose to LID (60).

The present results have major implications to both understanding the striatal pathophysiology of PD and developing novel therapeutic options. On one hand, our data point to D1-mGlu5 signaling complexes as mediators of maladaptive synaptic and molecular changes during the pharmacotherapy of PD (reviewed in (7, 8)). On the other hand, we here identify a novel mechanistic target for the treatment and prevention of LID, that is, a D1-mGlu5-dependent activation of PLC signaling. Indeed, we show that a pharmacological inhibition of PLC dampens the striatal activation of ERK1/2 and significantly improves dyskinesias induced by either L-DOPA or D1-like agonists without affecting the beneficial anti-akinetic effect of these treatments. We furthermore show that a genetic knockdown of mGlu5 in D1-positive neurons occludes the effect of both PLC and mGlu5 inhibition on dyskinesias evoked by either L-DOPA or a D1 receptor agonist. These data reveal the cell type in which D1-mGlu5 heteromers become pathophysiologically significant.

In line with the recent identification of GPCR heteromers as novel functional units and potential drug targets (46, 61), the present dissection of the D1-mGlu5 heteromer biochemical fingerprint could prompt a development of novel screening tools and ligands for therapeutic

research. Compared to the antagonists of ubiquitous D1 or mGlu5 receptors, compounds disrupting the D1-mGlu5 heteromer are predicted to offer a better risk-benefit profile for the treatment and prevention of LID.

Material and Methods

cDNA expression vectors. For BRET experiments, receptors were tagged at their extracellular N-terminus or intracellular C-terminus part using standard molecular biology techniques employing PCR and fragment replacement strategies resulting in plasmids coding for Rluc8-mGlu5a, Venus-D1, mGlu5a-Nluc and D1-Venus. The pRK5-HA-SNAP-mGlu5 plasmid was previously described (28). pRK5-HA-SNAP-mGlu5-DelCtail encodes for the mGlu5a receptor without C-terminal tail (until the GKSVT sequence at position 804). pRK5-cherryThr-CD4-mGlu5aCtail was obtained by substitution of mGlu1 C-tail coding sequence by mGlu5 C-tail coding sequence in the previously described pRK5-cherryThr-CD4-mGlu1Ctail plasmid (62). For Bimolecular Fluorescence Complementation, plasmids coding for D1-V1, D1-V2, CD8-V1 and CD8-V2 were generously given by J. Javitch (Columbia University, NY). The splits of monomeric Venus were fused to the C-terminus of the D1, mGlu5a or CD8. D1–V1 and CD8-V1 encode the N-terminal split of mVenus (1–155) fused to the D1 or CD8 respectively. D1–V2 and CD8-V2 express D1 receptor and CD8 respectively fused to C-terminal split of mVenus (156–240). The cDNA sequences coding for the splits of mVenus were amplified by PCR and subcloned in frame to the 3'-end coding sequence of mGlu5a without STOP codon in the pcDNA3.1-Myc-mGlu5a-Rluc8 plasmid to obtain plasmids coding for 5a-V1 and 5a-V2. The pmRFP plasmid coding for a MyrPalm tag corresponding to the N-terminal amino acid sequence (MGCIKSKRKDNLNDDE) from Lyn kinase fused to RFP protein was a kind gift from L. Hunday (Semmelweis University, Hungary). pGloSensor™ 22F-cAMP plasmid was from Promega and GcAMP6 coding plasmid was from Addgene.

Reagents. Coelenterazine H, Furimazine and D-luciferin were obtained from Promega. Drugs were purchased from Tocris and used at the following concentrations (except when indicated): DHPG: (S)-3,5-Dihydroxyphenylglycine (100 µM), SKF-81297: (±)-6-Chloro-2,3,4,5-tetrahydro-1-phenyl-1H-3-benzazepine hydrobromide (10 µM), MTEP: 3-((2-Methyl-1,3-

thiazol-4-yl)ethynyl)pyridine hydrochloride (10 µM), L-Quisqualic acid (10 µM), LY341495: (2S)-2-Amino-2-[(1S,2S)-2-carboxycycloprop-1-yl]-3-(xanth-9-yl) propanoic acid (100 µM).

Cell culture and transfection. Human embryonic kidney 293 cells (HEK293) cell culture and calcium phosphate precipitation method were previously described (15). The double stable HEK cell line co-expressing the Glo cAMP-sensor and the GcAMP6 Ca^{2+}-sensor was created in HEK293 cells. Double antibiotic-resistant clones were selected with 250 µg/ml hygromicyn + 500 µg/ml geneticin. Double-sensor stable cell line was plated in 96-well plates and transfected using Lipofectamine 2000 according to manufacturer's instruction (Sigma Aldrich). To maintain a low concentration of ambient glutamate, cells were co-transfected with the glutamate transporter EAAC1 and incubated in serum-free DMEM Glutamax Medium (Life Technologies) at least 2 hours before the different assays were performed.

Primary hippocampal neurons culture. Hippocampal neuronal primary cultures were prepared from embryonic day 17.5 rats as previously described (63). Briefly, brain hippocampi were digested with trypsin and hippocampal cells were seeded in neurobasal medium (NB) (Gibco, Invitrogen, Cergy Pontoise, France) supplemented with 2% B-27 (Gibco), 4 mM Glutamax (Gibco), 0.5 mM L-glutamine (Gibco), 100 U/ml Penicillin and 100 µg/ml Streptomycin and 10% Horse Bovine Serum, in 35mm diameter glass bottom culture dishes (MatTek Corporation, Ashland, MA, USA). After 1 day in vitro (DIV 1), the medium was replaced by serum-free neurobasal medium supplemented with 2% B-27, 0.5 mM Glutamax (Gibco) and antibiotics. Cells were incubated at 37°C, 5% CO2, 90% humidity. Hippocampal neurons were transfected according to the calcium phosphate transfection procedure previously described (64).

Bimolecular Fluorescence Complementation assay (BiFC). HEK cells were co-transfected with a 1:1 ratio of Venus splits V1 and V2 fusion proteins together with the pmRFP plasmid coding for a red fluorescent tag targeted to plasma membrane. 24 hours after transfection, cells were washed with PBS, fixed with 4% paraformaldehyde for 15 min. Cell nuclei were stained with DAPI and coverslips were mounted in Mowiol. Images were acquired using an Axio Observer Z.1 microscope and analyzed using Image J software. Red fluorescence images were thresholded to keep only plasma membrane fluorescence area. The selection corresponding to this threshold was transferred on the Venus fluorescence images and membranous

fluorescence of complemented Venus was quantified in this area. Intracellular fluorescence was measured in a square intracellular area excluding the nucleus. Membrane / (membrane + intracellular) Venus fluorescence ratio was then calculated and expressed as a percentage of total fluorescence.

Cell population BRET measurements. BRET measurements in cell populations were performed as previously described (65) using the Mithras LB 940 (Berthold Technologies). Briefly, HEK cells were transfected with a constant amount of the plasmid coding for the donor entity (1 µg of Rluc8-tagged donors or 100 ng of Nluc-tagged donors) combined with increasing quantities of the plasmid coding for the acceptor entity (0-4 µg). Suitable amount of the non-coding plasmid pcDNA3 was added to reach a total amount 5 µg of DNA per 100 mm dish. 48 hours after transfection, cells were suspended in PBS with 0.1% (w/v) glucose at room temperature (RT). Cells were then distributed in 96-well micro plates (Greiner) at a density of 100,000 cells/well with Rluc8 donor or 50,000 cells/well with Nluc donor. Before the BRET experiment, we measured the light emitted at 525 nm upon light excitation at 485 nm, indicative of the amount of Venus-tagged proteins. BRET (535 nm / 485 nm ratio) was assessed by calculating the ratio of the light emitted by the acceptor entity (510-550 nm band-pass filter, Em535) to the light emitted by the donor (460–500 nm band-pass filter, Em480) after the addition of 5 µM of the Rluc8 substrate, Coelenterazine H or 20 µM of the Nluc substrate, Furimazine. Net BRET values were plotted as a function of total fluorescence/luminescence ratio and saturation curves were drawn using the "one-site specific binding non-linear" fit of GraphPad Prism 7 software (GraphPad Software Inc.)

Single-cell BRET imaging. Single-cell BRET imaging experiments were performed and analyzed as previously described (43, 66, 67). Briefly, hippocampal neurons in culture were co-transfected at DIV10 to 12 either with plasmids coding for the Nluc-tagged donor together with the Venus-tagged acceptor or with plasmids coding for the donor only and DsRed as a transfection reporter. 24 to 48-hours after transfection, neurons were recorded in the following external medium: 140 mM NaCl, 2 mM CaCl2, 3 mM KCl, 10 mM Hepes, 10 mM d-glucose, 0.01 mM glycine, pH 7.4, with an osmolarity of 330 mOsm.

TR-FRET measurements. TR-FRET experiments with the SNAP-tagged mGlu5 receptor was performed as previously described for others mGluRs (28). HEK293 cells were co-transfected

with plasmids coding for HA-SNAP-mGlu5 with or without D1-Venus. 24-hours after transfection, cells were incubated at 37 °C for 1 hour with a solution of 100 nM of SNAP-Lumi4-Tb and 60 nM of SNAP-Green in Tag-Lite buffer (Cisbio). After being labeled, cells were washed three times with Tag-Lite, and indicated drugs were added at final concentrations indicated in the figure legend. The TR-FRET measurements were performed using a PHERAstar FS microplate reader (BMG Labtech, Germany). To monitor the emissive decay curves, the Lumi4-Tb present in each well was excited using N_2 laser emission line at 337 nm. The emission decay was collected during 2500 with 5 µs steps, respectively, at 620 nm for the donor (Lumi4-Tb) and at 520 nm for Green. The acceptor ratio was calculated using the acceptor signal integrated over the time window [50 µs-100 µs], divided by the acceptor signal integrated over the time window [400 µs-800 µs].

InsP assay in cells. Quantification of InsP levels were performed using the Homogeneous Time-Resolved FRET (HTRF) assay IPone kit according to the manufacturer's recommendations (Cisbio, Bedord, USA). HEK cells were plated in 96-well plates and transiently transfected with the indicated receptors together with the glutamate transporter EAAC1. The day of the experiments, cells were incubated for 2 hours in serum-free DMEM Glutamax before stimulation with mGlu5 ligands for 30 min at 37°C (L-Quisqualic acid (10 µM) or LY341495 (100 µM). Cells were then lysed using the supplied lysis buffer containing d2-labeled InsP and Lumi4-Tb^{TM} cryptate-labeled anti-InsP antibodies. The HTRF signal was measured after 1h RT incubation in the dark using PHERAstar FS microplate reader. FRET signal was determined by measuring d2 acceptor emission (665 nm) and Tb donor emission (620 nm) using a 50 µs delay and a 450 µs integration upon excitation at 337 nm on a PHERAstar FS (BMG LabTech, Ortenberg, Germany). TR-FRET (or HTRF) ratio (665 nm/620 nm × 10^4, Cisbio Bioassays patent US5,527,684) was calculated.

Intracellular Calcium and cAMP measurements. After 2-hours in serum-free DMEM Glutamax, stable double-sensor HEK cells were washed with Tag-Lite. Drug-triggered cytosolic calcium release was monitored by measurements of GcAMP6 fluorescence (excitation 485 nm and emission 525 nm) using a FlexStation (Molecular Devices, USA). Increasing drug concentrations were injected after 20 seconds of recording. For basal controls, buffer alone was added after 20s. For cAMP measurement, the GloSensor^{TM} (Promega) assay is based on cAMP-induced conformational changes of a genetically-modified firefly luciferase into which

a cAMP-binding protein moiety has been inserted. Cells were incubated in Tag-Lite buffer with 450µg/mL of D-Luciferin during 1 hour at RT in the dark. After 5-min of temperature stabilization at 28°C in the plate-reader, increasing doses of ligand were added to the cells with 500 µM of IBMX (cAMP/cGMP phosphodiesterases inhibitor). Drug-triggered cAMP production was assessed by luminescence measurements using Mithras LB 940 plate-reader (no emission filter, 1s-integration time). For each drug concentration, the maximal amplitude of fluorescence or luminescence intensity increase was plotted with respect to the concentrations in a logarithmic scale. Dose-response curves were drawn using the "log (agonist) vs response (three parameters)" non-linear fit of GraphPad Prism 7 software (GraphPad Software Inc.).

Proximity ligation assay. Experiments were performed on intact and lesioned striatal sections of both Wt and *mGluR5*$^{KO\text{-}D1}$ mice following a period of daily s.c. treatment with either vehicle or L-DOPA (6 mg/kg) for 3 weeks. Coronal striatal sections, 50 µm thick, were blocked with 10 % horse serum and permeabilized with 0.2% Triton X-100 (v/v). Experiments were then performed according to the manufacturer's instructions (Duolink® & PLA® Technology, Olink-Bioscience, Uppsala, Sweden, (44)). Briefly, sections were incubated with D1 guinea-pig primary antibodies (Frontier Institut Co., ltd. AB_2571595) directly conjugated to minus Duolink II PLA probes and with mGlu5 rabbit primary antibody (Millipore. AB5675) at 4°C for 36-48 hours. PLA probes anti-rabbit plus, which are secondary antibodies conjugated with oligonucleotides, were added and incubated for 1 h at 37°C. Amplification template oligonucleotides were hybridized to pairs of PLA and circularized by ligation. The hence formed DNA circle was then amplified using rolling circle amplification and detection of the amplicons was carried out using the 624 Duolink in situ detection kits, resulting in red fluorescence signals. Sections were mounted and were analyzed under a 40X oil immersion objective using a confocal microscope (Zeiss LSM 780 or Leica TCS SP8 X). All acquisitions were made the same day under the same microscope setting and laser power to minimize variability among samples. Distinct bright spots contained within an area of the section designated by the experimenter were counted using an ImageJ macro. Briefly, we determined a pre-sized zone of interest (ROI) and then performed segmentation by thresholding in order to generate binary images. Six ROIs were analyzed per striatum to measure a mean value per animal. To minimize experimental bias during the analysis, all images were processed blindly using the

intermodes autothreshold function (68). With this approach, we observed minimum variability in the analysis of PLA quantification. Using the Analyze Particle function of ImageJ, the numbers of particles larger than 0.198 µm2 in the binary image were counted as clusters. Data were exported to Prism software for further analysis.

Animals. Behavioural experiments were performed using female Sprague Dawley rats (200-225 g; Charles River, Denmark), or wildtype mice and bacterial artificial chromosome (BAC) transgenic mice having a selective knockdown of mGlu5 in D1 receptor-expressing neurons (the previously characterised *mGluR5*$^{KD\text{-}D1}$ line (9,11)). For studying receptor complexes (Figure 6) and SKF38393-induced pERK1/2 activation (Figure 7G-H), we used mice with a genetic ablation of the mGlu5 receptor in D1-expressing cells, obtained by crossbreeding homozygous mGluR5$^{loxP/loxP}$ mice (69) with heterozygous BAC-Drd1a-Cre mice (GENSAT project founder line EY262 (70). All mice were on a C57BL/6 genetic background and approximately 10 weeks old at the beginning of the experiments; both sexes were used. Rats and mice were housed under a 12-h light/dark cycle with access to water and food ad libitum.

Dopamine-denervating lesions. Unilateral DA-denervating lesions were produced by injecting 6-hydroxydopamine (6-OHDA) in the right medial forebrain bundle (MFB), according to methods that are well established in both in rats and mice (71, 72). Mice were anesthetized using a mixture of 4% isofluorane in air (Isobavet, Apoteksbolaget) and placed in a stereotaxic frame with a mouse adaptor (Kopf Instruments, Tujunga, USA) on a flat skull position. The toxin 6-OHDA-HCl (Sigma Aldrich, Stockholm, Sweden) was dissolved in a 0.02% ascorbic acid-saline solution (3.2 µg free base 6-OHDA/µl) and 1 µl was injected with a glass capillary attached to a 10 µl Hamilton syringe at the following coordinates (in mm, relative to bregma and dural surface): AP = −0.7, L = −1.2, DV = −4.7. The injection rate was 0.5 µl/min, and the capillary was left in place for 2 min before and 2 min after the injection. The analgesic Marcain (bupivacaine, 2.5 mg/ml, AstraZeneca) was injected subcutaneously (10 µl/10 g, body weight) before first skin incision. Postoperative care of the mice was performed as in (73). Rats were anesthetized with a mixture of Fentanyl and Dormitor (20:1; Apoteksbolaget, Sweden AB) and placed in a stereotactic frame (Kopf Instruments, Tujunga, USA). The toxin solution was prepared as for the mouse and injected at the following coordinates (in mm, relative to bregma and dural surface): first injection: A = −4.4, L = −1.2, V = −7.8, tooth bar = +2.4 (2,5 µl);

second injection: A = −4.0, L = −0.8, V = −8.0, tooth bar = +3.4 (2,0 µl). After surgery, animals received an analgesic treatment with Temgesic (Apoteksbolaget AB, Sweden).

Evaluation of 6-OHDA lesion in mice and rats. Three weeks after 6-OHDA lesion, forelimb use asymmetry was evaluated in rats and mice using the 'cylinder test', revealing a significant reduction in the spontaneous use of the forelimb contralateral to the lesion (71–74). Briefly, mice and rats were placed individually in a glass cylinder (10 cm diameter and 14 cm height for mice; 21 cm diameter and 34 cm height for rats) and were videotaped for 5 min. The total number of supporting wall contacts performed independently with left and right forepaw were counted off-line. Results were expressed as the percentage use of the forelimb contralateral to the lesion [left forepaw contact/total number of wall contacts)*100]. The 6-OHDA-lesioned animals used in this study were selected using a stringent cut-off value of ≤ 25% contralateral paw usage. The cylinder test was also used to evaluate beneficial "therapeutic-like" effects of L-DOPA and rule out possible adverse effects by U73122 (rat data in Suppl Figs. S2, mouse data in Suppl Fig S3). To assess the anti-akinetic action of L-DOPA, animals were recorded at 15-20 min post L-DOPA injection. In addition to the behavioural screening, tyrosine hydroxylase histochemistry was used to verify the extent of nigrostriatal DA degeneration at the end of the experiments (see below).

In vivo drug treatments. L-DOPA methyl ester (3 and 6 mg/kg, Sigma Aldrich AB, Sweden) was always coadministered with a fixed dose of Benserazide-HCl (12 mg/kg in both rats and mice; Sigma Aldrich AB, Sweden). The drugs were freshly dissolved in physiological saline and injected s.c.. All other drugs used, their doses and administration modalities in vivo are reported in Supplemental Table 1.

Abnormal involuntary movements (AIMs) ratings. Mice and rats were individually placed in transparent plastic cages and allowed to habituate for at least 2 hours before the first test, and for 15 min before each subsequent test. Abnormal involuntary movements (AIMs) were quantified by an experimentally blinded investigator using previously validated scales (73–75). Briefly, each animal was rated online for 1 min every 20 min for up to 200 min following the injection of a DAergic agent. Three topographic subtypes of dyskinesia were considered: (i) axial AIMs (twisting of the neck and upper trunk towards the side contralateral to the lesion), (ii) forelimb AIMs (purposeless movements or dystonic posturing of the contralateral

forelimb), (iii) orolingual AIMs (facial/jaw movements and contralateral tongue protrusion). These three AIM subtypes were scored simultaneously on two severity scales (each graded from 0 to 4), one based on the proportion of observation time during which dyskinetic movements were present, the other one based on movement amplitude (i.e. degree of deviation of the dyskinetic body part from its natural resting position). Time-based severity scores were multiplied by the amplitude scores for each subtype and observation point, and the sum of these products was used in the final analysis. The sum of AIM scores between 40 and 80 min after the injection of a DAergic agent was defined as "peak-AIMs" in agreement with previous studies (38, 39, 75).

Open field: This test was used as a part of the phenotypic characterization of *mGluR5*$^{KD\text{-}D1}$ mice after the lesion (see Suppl. Figure S4). Mice were monitored in an open field using a video-tracking system (Stoelting ANY-MAZE video tracking) that detects the position of the animal's head, body, and tail in the arena (transparent Plexiglas boxes of 50 x 50cm). The system provides measures of spontaneous horizontal activity (distance travelled) and turning movements (based on the rotation of the mouse body axes) expressed as the number of clockwise and anticlockwise full turns. Each recording session lasted 160 min and data were expressed as total distance travelled (in meters) and total number of ipsi- or contralateral turns.

Immunohistochemistry. Rats and mice were anaesthetized with pentobarbital (240 mg/kg, i.p., Apoteksbolaget AB, Sweden) 30 min after the final injection of either L-DOPA or SKF38393 and were transcardially perfused with 4% ice-cold PFA (pH 7.4). Extracted brains were postfixed in 4% ice-cold PFA for 2 hours and subsequently transferred to a 25% sucrose solution for 24-36 hours. Brains were sectioned coronally on a freezing microtome at 30 µm thickness. Free-floating sections from the striatum were used for immunohistochemical detection of phosphorylated ERK (pERK1/2) and tyrosine hydroxylase (TH). Briefly, sections were blocked for 1 hour in 5% normal goat serum in Tris-buffered saline and were incubated for 24-48 hours with one of the following primary antibodies: rabbit-anti-phospho$^{Thr202/Tyr204}$ ERK1/2 (#9101; Cell Signaling Technology, 1:250; rabbit-anti-TH (#P40101; Pel-Freeze, Rogers, AR, 1:1000). Sections were then rinsed and incubated in 2.5% serum blocking solution containing biotinylated goat-anti-rabbit antibodies (BA1000; Vector Laboratories, Burlingame, CA, U.S.A., 1:200). Immunocomplexes were visualized using a standard avidin-biotin-

peroxidase complex (Vectastain Elite ABC-kit; Vector Laboratories, Burlingame, CA, U.S.A.) with 3'3'-diaminobenzidine (DAB; Sigma Aldrich, Sweden) as the chromogen. Slide-mounted sections were dehydrated and coverslipped with DPX mounting medium (Sigma Aldrich, Sweden).

Counts of pERK1/2-positive cells. Striatal sections immunostained for pERK1/2-were visualised under a 20x objective using a Nikon eclipse 80i microscope merged with a Nikon DMX 1200F video camera (11). Sample areas (0.913 mm^2) were acquired from the dorsomedial (DM) and ventrolateral (VL) quadrants of the motor striatum at three different coronal levels (rostral, mid, and caudal striatum) based on predefined anatomical coordinates. In each dataset to be compared, all acquisitions were made on the same day under the same microscope setting. The digitised images were then converted to a 8-bit greyscale using the open source image processing program ImageJ (NIH). Background threshold was set to the same value in all samples, and immunostained cells were counted as single particles in an automated fashion ("analyse particles" plugin). Data were expressed as total number of immunoreactive cells per sample area (averaged for all sample areas per striatal quadrant per animal).

InsP assay in striatal slices. InsP formation was measured in rat striatal slices pre-labeled with a tritiated precursor as described in (32). A total of twenty rats with unilateral 6-OHDA lesions were sacrificed by decapitation; striatal tissue was manually dissected out on ice and transferred on ice-cold Krebs-Henseleit buffer (NaCl 118 mM, KCl 4.7 mM, $MgSO_4$ 1.18 mM, KH_2PO_4 1.18 mM, $NaHCO_3$ 24.8 mM, $CaCl_2$ 1.2 mM, D-glucose 10 mM) that had been pre-gassed with 95% O2 and 5% CO2 to pH 7.4. Slices (350 x 350 μm) were prepared using a Mc Ilwain tissue chopper and randomly distributed into different tubes. Forty μl of gravity packed slices/tube were incubated for 60 min in 350 μl buffer containing 1 μCi of myo-[^{3}H]inositol. Slices were then incubated with LiCl (10 mM; to block InsP degradation) and with the mGlu1 receptor antagonist JNJ16259685 (10 μM; to block mGlu1 receptors). Thereafter, slices were stimulated with ligands of D1 and mGlu5 receptors at standard concentrations for this assay (76-77). The following treatments were compared: (i) vehicle (basal levels), (ii) the D1 receptor agonist SKF38393 (200 μM), (iii) the group I mGlu receptor agonist DHPG (200 μM), (iv) the combination of SKF38393 and DHPG, and (v) the same combination as in (iv) in the

presence of the mGlu5 antagonist MTEP (10 μM). Incubations were stopped after 60 min by adding 900 μl methanol:chloroform (2:1). After further addition of 300 μl chloroform and 600 μl water, samples were centrifuged at low speed to facilitate phase separation and the [^{3}H]InsP present in the supernatant was separated by anion exchange chromatography. Samples were removed from their water phase, incubated with 0.5 N NaOH and let to dry at 50 °C for 2 hours. Proteins were measured as described by Lowry et al. (78). In the statistical analysis, n represents the number of tubes incubated with different treatments (each tube containing tissue from more than 1 rat, as in (32).

Statistical analysis. Statistical analysis was carried out using GraphPad Prism 7 software (GraphPad Software Inc.). Statistical tests and *post-hoc* comparisons are indicated in the figure legends. Values of $p<0.05$ were considered statistically significant. Data compared using parametric statistical tests are presented as group mean ± SEM, whereas data compared with non-parametric statistics are presented as group median and range.

Acknowledgements

This work was supported by the European Research Council (ERC) under the European Union's Horizon 2020 research and innovation program (JP, grant agreement No. 646788), the Agence Nationale de la Recherche (JP, ANR-13-JSV4-0005-01 and ANR-17-CE11-0046) and the Région Languedoc-Roussillon (Chercheur d'Avenir) to JP; by grants from the Swedish Research Council, the Basal Ganglia Disorders Linnaeus Consortium (BAGADILICO), the Swedish Brain Foundation, and the Swedish Governmental Funds for Clinical research to MAC. IS is supported by a post-doctoral scholarship from the Swedish Brain Foundation. We thank Dr. Javitch (Columbia University, NY, USA) for providing us the Venus-split plasmids, Dr. Gales (Toulouse University, France) for providing the Nluc-Gαq plasmid and Dr. Hunday (Semmelweis University, Hungary) for giving us the pmRFP plasmid. We thank the Arpege platform (IGF, Montpellier) for the use of fluorimeters for cell-population BRET and functional assays, and Ann-Christin Lindh, Elena Espa, and Michael Sparrenius for excellent technical assistance.

Author Contributions

IS, EG, MAC and JP designed the experiments, analyzed and interpreted the data, and wrote the manuscript. IS performed all experiments in rats with the assistance of NM (behavioral pharmacology) and LDM (InsP hydrolysis assay). IS and LA performed behavioral-pharmacological and histopathological experiments in mice; EG performed most of the experiments on the physical and functional molecular interaction *in vitro*. DM & JFI designed, performed and analyzed the TR-FRET experiments and helped with the pharmacological data analysis. NB helped to the conception and production of Venus and Luciferase fusion BRET probes. EM performed BRET experiments in HEK cells. FA designed, performed and analyzed the PLA experiments. CJ-T performed PLA experiments. LA, J-PP, LF, and FN provided help with experiment design, data analysis and interpretation to different parts of the study.

Conflict of interest:

The authors have no relevant conflict of interest to declare.

References

1. Pisani A, Centonze D, Bernardi G, Calabresi P. Striatal synaptic plasticity: Implications for motor learning and Parkinson's disease. *Mov. Disord.* 2005;20(4):395–402.

2. Maia T V., Frank MJ. From reinforcement learning models to psychiatric and neurological disorders. *Nat. Neurosci*. 2011; 14(2):154–162

3. Redgrave P et al. Goal-directed and habitual control in the basal ganglia: Implications for Parkinson's disease. *Nat. Rev. Neurosci.* 2010;11(11):760–772.

4. Bagetta V, Ghiglieri V, Sgobio C, Calabresi P, Picconi B. Synaptic dysfunction in Parkinson's disease. *Biochem Soc Trans* 2010;38(2):493–497.

5. Fiorentini C et al. Loss of synaptic D1 dopamine/N-methyl-D-aspartate glutamate receptor complexes in L-DOPA-induced dyskinesia in the rat. *Mol. Pharmacol.* 2006;69(3):805–812.

6. Picconi B et al. Loss of bidirectional striatal synaptic plasticity in L-DOPA-induced dyskinesia. *Nat. Neurosci.* 2003;6(5):501–506.

7. Cenci MA, Konradi C. Maladaptive striatal plasticity in l-DOPA-induced dyskinesia. *Prog Brain Res*. 2010; 183:209–233.

8. Murer MG, Moratalla R. Striatal signaling in L-DOPA-induced dyskinesia: Common mechanisms with drug abuse and long term memory involving D1 dopamine receptor stimulation. *Front. Neuroanat.* 2011;5:51.

9. Novak M et al. Incentive learning underlying cocaine-seeking requires mGluR5 receptors located on dopamine D1 receptor-expressing neurons. *J. Neurosci.* 2010;30(36):11973–11982.

10. Sebastianutto I, Cenci MA. mGlu receptors in the treatment of Parkinson's disease and L-DOPA-induced dyskinesia. *Curr. Opin. Pharmacol.* 2018;38:81–89.

11. Fieblinger T et al. Mechanisms of dopamine D1 receptor-mediated ERK1/2 activation in the parkinsonian striatum and their modulation by metabotropic glutamate receptor type 5. *J. Neurosci.* 2014;34(13):4728–4740.

12. Dacres H, Wang J, Dumancic MM, Trowell SC. Experimental determination of the förster distance for two commonly used bioluminescent resonance energy transfer pairs. *Anal. Chem.* 2010;82(1):432–435.

13. Juhasz JR et al. Mu-opioid receptor heterooligomer formation with the dopamine D1 receptor as directly visualized in living cells. *Eur. J. Pharmacol.* 2008;581(3):235–243.

14. Lee FJS et al. Dual regulation of NMDA receptor functions by direct protein-protein interactions with the dopamine D1 receptor. *Cell* 2002;111(2):219–230.

15. Perroy J et al. Direct interaction enables cross-talk between ionotropic and group I metabotropic glutamate receptors. *J Biol Chem* 2008;283(11):6799–6805.

16. Abe T et al. Molecular characterization of a novel metabotropic glutamate receptor mGluR5 coupled to inositol phosphate/Ca2+ signal transduction. *J. Biol. Chem.* 1992;267(19):13361–13368.

17. Lei S. Cross interaction of dopaminergic and adrenergic systems in neural modulation. *Int. J. Physiol. Pathophysiol. Pharmacol.* 2014;6(3):137–142.

18. Smith Y, Charara A, Hanson JE, Paquet M, Levey AI. GABA(B) and group I metabotropic glutamate receptors in the striatopallidal complex in primates. *J. Anat.* 2000;196(4):555–576.

19. Gubellini P, Pisani A, Centonze D, Bernardi G, Calabresi P. Metabotropic glutamate receptors and striatal synaptic plasticity: Implications for neurological diseases. *Prog. Neurobiol.* 2004;74(5):271–300.

20. Dickerson JW, Conn PJ. Therapeutic potential of targeting metabotropic glutamate receptors for Parkinson's disease. *Neurodegener. Dis. Manag.* 2012;2(2):221–232.

21. Vidi PA, Przybyla JA, Hu CD, Watts VJ. Visualization of G protein-coupled receptor (GPCR) Interactions in living cells using bimolecular fluorescence complementation (BiFC). *Curr. Protoc. Neurosci.* 2010;Ch.5:Unit 5.29

22. Jaeger WC, Armstrong SP, Hill SJ, Pfleger KDG. Biophysical detection of diversity and bias in GPCR function. *Front. Endocrinol. (Lausanne).* 2014;5:26.

23. Ladepeche L et al. Single-molecule imaging of the functional crosstalk between surface NMDA and dopamine D1 receptors. *Proc. Natl. Acad. Sci. U. S. A.* 2013;110(44):18005–18010.

24. Kern A et al. Hippocampal Dopamine/DRD1 Signaling Dependent on the Ghrelin Receptor. *Cell* 2015;163(5):1176–1190.

25. Luján R, Nusser Z, Roberts JDB, Shigemoto R, Somogyi P. Perisynaptic location of metabotropic glutamate receptors mGluR1 and mGluR5 on dendrites and dendritic spines in the rat hippocampus. *Eur. J. Neurosci.* 1996;8(7):1488–1500.

26. Sesack SR, Aoki C, Pickel VM. Ultrastructural localization of D2 receptor-like immunoreactivity in midbrain dopamine neurons and their striatal targets.. *J. Neurosci.* 1994;14(1):88-106.

27. Liu XY et al. Modulation of D2R-NR2B Interactions in Response to Cocaine. *Neuron* 2006;52(5):897–909.

28. Doumazane E et al. Illuminating the activation mechanisms and allosteric properties of metabotropic glutamate receptors. *Proc. Natl. Acad. Sci. U. S. A.* 2013;110(15):E1416-25

29. Nasrallah C et al. Direct coupling of detergent purified human mGlu5 receptor to the heterotrimeric G proteins Gq and Gs. *Sci. Rep.* 2018;8(1).

30. Urizar E et al. CODA-RET reveals functional selectivity as a result of GPCR heteromerization. *Nat. Chem. Biol.* 2011;7(9):624–630.

31. Pin JP, Duvoisin R. Review: Neurotransmitter receptors I. The metabotropic glutamate receptors: Structure and functions. *Neuropharmacology* 1995;34(1):1–26.

32. Nicoletti F et al. Coupling of Inositol Phospholipid Metabolism with Excitatory Amino Acid Recognition Sites in Rat Hippocampus. *J. Neurochem.* 1986;46(1):40–46.

33. De La Fuente-Fernández R et al. Levodopa-induced changes in synaptic dopamine levels increase with progression of Parkinson's disease: Implications for dyskinesias. *Brain* 2004;127(12):2747–2754.

34. Ahmed I et al. Glutamate NMDA receptor dysregulation in Parkinson's disease with dyskinesias. *Brain* 2011;134(4):979–986.

35. Fasano S et al. Inhibition of Ras-guanine nucleotide-releasing factor 1 (Ras-GRF1) signaling in the striatum reverts motor symptoms associated with L-dopa-induced dyskinesia. *Proc. Natl. Acad. Sci. U. S. A.* 2010;107(50):21824–21829.

36. Westin JE, Vercammen L, Strome EM, Konradi C, Cenci MA. Spatiotemporal Pattern of Striatal ERK1/2 Phosphorylation in a Rat Model of L-DOPA-Induced Dyskinesia and the Role of Dopamine D1 Receptors. *Biol. Psychiatry* 2007;62(7):800–810.

37. Rylander D et al. Pharmacological modulation of glutamate transmission in a rat model of L-DOPA-induced dyskinesia: Effects on motor behavior and striatal nuclear signaling. *J. Pharmacol. Exp. Ther.* 2009;330(1):227–235.

38. Rylander D et al. A mGluR5 antagonist under clinical development improves L-DOPA-induced dyskinesia in parkinsonian rats and monkeys. *Neurobiol. Dis.* 2010;39(3):352–361.

39. Iderberg H, Rylander D, Bimpisidis Z, Cenci MA. Modulating mGluR5 and 5-HT1A/1B receptors to treat l-DOPA-induced dyskinesia: Effects of combined treatment and possible mechanisms of action. *Exp. Neurol.* 2013;250:116–124.

40. Delfino MA et al. Behavioral sensitization to different dopamine agonists in a parkinsonian rodent model of drug-induced dyskinesias. *Behav. Brain Res.* 2004;152(2):297–306.

41. Ding Y et al. Enhanced striatal cholinergic neuronal activity mediates L-DOPA-induced dyskinesia in parkinsonian mice. *Proc. Natl. Acad. Sci. U. S. A.* 2011;108(2):840–845.

42. Foster DJ, Conn PJ. Allosteric Modulation of GPCRs: New Insights and Potential Utility for Treatment of Schizophrenia and Other CNS Disorders. *Neuron* 2017;94(3):431–446.

43. Goyet E, Bouquier N, Ollendorff V, Perroy J. Fast and high resolution single-cell BRET imaging [Internet]. *Sci Rep* 2016;6:28231.

44. Fredriksson S et al. Protein detection using proximity-dependent DNA ligation assays. *Nat. Biotechnol.* 2002;20(5):473–477.

45. Pavón N, Martín AB, Mendialdua A, Moratalla R. ERK phosphorylation and FosB expression are associated with L-DOPA-induced dyskinesia in hemiparkinsonian mice. *Biol. Psychiatry* 2006;59(1):64–74.

46. Borroto-Escuela DO et al. Understanding the role of gpcr heteroreceptor complexes in modulating the brain networks in health and disease. *Front. Cell. Neurosci.* 2017;11:37.

47. Cerovic M et al. Derangement of ras-guanine nucleotide-releasing factor 1 (Ras-GRF1) and extracellular signal-regulated kinase (ERK) dependent striatal plasticity in L-DOPA-Induced dyskinesia. *Biol. Psychiatry* 2015;77(2):106–115.

48. Heiman M et al. Molecular adaptations of striatal spiny projection neurons during levodopa-induced dyskinesia. *Proc. Natl. Acad. Sci. U. S. A.* 2014;111(12):4578–4583.

49. Santini E, Heiman M, Greengard P, Valjent E, Fisone G. Inhibition of mTOR signaling in parkinson's disease prevents L-DOPA-induced dyskinesia. *Sci. Signal.* 2009;2(80):ra36.

50. Girault JA, Valjent E, Caboche J, Hervé D. ERK2: a logical AND gate critical for drug-induced plasticity?. *Curr. Opin. Pharmacol.* 2007;7(1):77–85.

51. Valjent E et al. Involvement of the extracellular signal-regulated kinase cascade for cocaine-rewarding properties. *J. Neurosci.* 2000;20(23):8701–8709.

52. Bouvier M. Oligomerization of G-protein-coupled transmitter receptors. *Nat. Rev. Neurosci.* 2001;2(4):274–286.

53. Doumazane E et al. A new approach to analyze cell surface protein complexes reveals specific heterodimeric metabotropic glutamate receptors. *FASEB J.* 2011;25(1):66–77.

54. Rives ML et al. Crosstalk between GABAB and mGlu1a receptors reveals new insight into GPCR signal integration. *EMBO J.* 2009;28(15):2195–2208.

55. Testa CM, Standaert DG, Young AB, Penney JB. Metabotropic glutamate receptor mRNA expression in the basal ganglia of the rat. *J. Neurosci.* 1994;14(5 II):3005–3018.

56. Beggiato S et al. Functional role of striatal A2A, D2, and mGlu5 receptor interactions in regulating striatopallidal GABA neuronal transmission. *J. Neurochem.* 2016;138(2):254–264.

57. Cabello N et al. Metabotropic glutamate type 5, dopamine D2 and adenosine A 2a receptors form higher-order oligomers in living cells. *J. Neurochem.* 2009;109(5):1497–1507.

58. Song L et al. Targeting the D1-N-methyl-D-aspartate receptor complex reduces L-dopa-induced dyskinesia in 6-hydroxydopamine-lesioned Parkinson's rats. *Drug Des. Devel. Ther.*

2016;10:547–555.

59. Farré D et al. Stronger Dopamine D1 Receptor-Mediated Neurotransmission in Dyskinesia. *Mol. Neurobiol.* 2015;52(3):1408–1420.

60. Nadjar A, Gerfen CR, Bezard E. Priming for l-dopa-induced dyskinesia in Parkinson's disease: A feature inherent to the treatment or the disease?. *Prog. Neurobiol.* 2009;87(1):1–9.

61. Fuxe K et al. Moonlighting proteins and protein-protein interactions as neurotherapeutic targets in the G protein-coupled receptor field. *Neuropsychopharmacology* 2014;39(1):131–155.

62. Raynaud F et al. SNAP23-Kif5 complex controls mGlu1 receptor trafficking. *J. Mol. Cell. Biol.* 2018;10(5):423-436.

63. Xu C et al. REV, A BRET-Based Sensor of ERK Activity. *Front Endocrinol* 2013;4:95.

64. Goetze B, Grunewald B, Baldassa S, Kiebler M. Chemically controlled formation of a DNA/calcium phosphate coprecipitate: Application for transfection of mature hippocampal neurons. *J. Neurobiol.* 2004;60(4):517–525.

65. Perroy J, Pontier S, Charest PG, Aubry M, Bouvier M. Real-time monitoring of ubiquitination in living cells by BRET. *Nat Methods* 2004;1(3):203–208.

66. Coulon V et al. Subcellular imaging of dynamic protein interactions by bioluminescence resonance energy transfer. *Biophys J* 2008;94(3):1001–1009.

67. Chastagnier Y, Moutin E, Hemonnot AL, Perroy J. Image processing for bioluminescence resonance energy transfer measurement-BRET-Analyzer. *Front. Comput. Neurosci.* 2018;11:118.

68. Prewitt JMS, Mendelsohn ML. the Analysis of Cell Images. *Ann. N. Y. Acad. Sci.* 1966;128(3):1035–1053.

69. Xu J, Zhu Y, Contractor A, Heinemann SF. MGluR5 has a critical role in inhibitory learning. *J. Neurosci.* 2009;29(12):3676–3684.

70. Gong S et al. Targeting Cre recombinase to specific neuron populations with bacterial artificial chromosome constructs. *J. Neurosci.* 2007;27(37):9817–9823.

71. Cenci MA, Lundblad M. Ratings of L -DOPA-Induced Dyskinesia in the Unilateral 6-OHDA Lesion Model of Parkinson's Disease in Rats and Mice. *Curr Prot Neurosci*. 2007; Ch.9:Unit 9.25.

72. Francardo V et al. Impact of the lesion procedure on the profiles of motor impairment and molecular responsiveness to L-DOPA in the 6-hydroxydopamine mouse model of Parkinson's

disease. *Neurobiol. Dis.* 2011;42(3):327–340.

73. Sebastianutto I, Maslava N, Hopkins CR, Cenci MA. Validation of an improved scale for rating L-DOPA-induced dyskinesia in the mouse and effects of specific dopamine receptor antagonists. *Neurobiol. Dis.* 2016;96:156–170.

74. Lundblad M et al. Pharmacological validation of behavioural measures of akinesia and dyskinesia in a rat model of Parkinson's disease. *Eur. J. Neurosci.* 2002;15(1):120–132.

75. Breger LS, Dunnett SB, Lane EL. Comparison of rating scales used to evaluate l-DOPA-induced dyskinesia in the 6-OHDA lesioned rat. *Neurobiol. Dis.* 2013;50(1):142–150.

76. Romano MR et al. Type-1, but Not Type-5, Metabotropic Glutamate Receptors are Coupled to Polyphosphoinositide Hydrolysis in the Retina. *Neurochem. Res.* 2016;41(4):924–932.

77. Di Menna L et al. Functional partnership between mGlu3 and mGlu5 metabotropic glutamate receptors in the central nervous system. *Neuropharmacology* 2018;128:301–313.

78. Bennett G. Lowry's handbook of right-to-know emergency planning. *J. Hazard. Mater.* 1992;30(3):361–362.

Figures and Figure legends

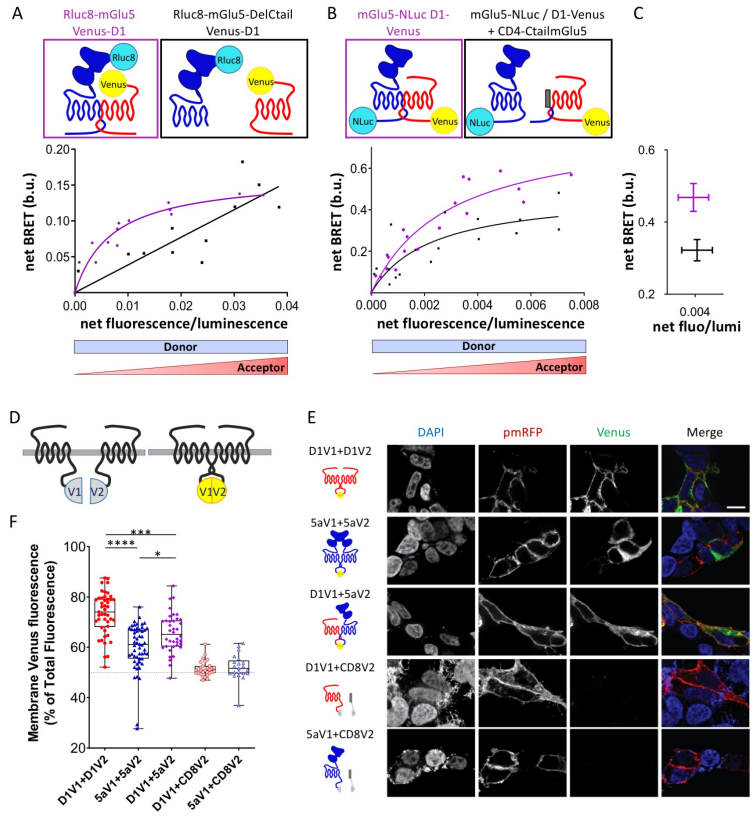

Figure 1 - Characterization of the heteromerization between mGlu5 and D1 receptors in living cells.
A- C – BRET titration curves were measured on HEK293 cells co-transfected with N- **(A)** or C-tagged **(B)** receptors. BRET signals were measured for increasing expression levels of acceptor (Venus-D1 **(A)** or D1-Venus **(B)**) at constant level of donor expression (Rluc8-mGlu5 **(A)** or mGlu5-Nluc **(B)**). Results were analyzed by nonlinear regression on a pooled data set from three independent experiments, assuming a model with one-site binding (GraphPad Prism 7). **A -** BRET signals were measured between Venus-D1 receptor and Rluc8-mGlu5 (purple curve) or Rluc8-mGlu5 deleted from its Ctail (Rluc8-mGu5-DelCtail, black curve). **B -** BRET signals were measured between D1-Venus and mGlu5-Nluc, with (black curve) or without (purple curve) co-expression of mGu5-Ctail fused to the CD4 membrane domain (CD4-CtailmGlu5). **C -** Decrease of the net BRET signal between D1-Venus and mGlu5-Nluc in cells co-expressing CD4-mGlu5Ctail (black) for identical D1-Venus / mGlu5-Nluc expression ratio. p=0.0571, Mann-Whitney test.
D-F – Bimolecular fluorescence complementation (BiFC) was measured on transiently transfected HEK293 cells. **D -** Schematic representation of BiFC principle. Non-fluorescent fragments from the Venus fluorescent protein (V1 and V2) are fused to putative interaction partners. Physical association of partners triggers bimolecular fluorescent Venus complex. **E -** BiFC images of receptors fused to non-fluorescent monomeric Venus split V1 or V2. Specificity was controlled in cells expressing D1-V1 or 5a-V1 together with CD8-V2 (last 2 lines). The green channel illustrates the expression of Venus complementation (V1 + V2), whereas DAPI and pmRFP fluorescences were used to stain the nucleus and plasma membrane, respectively. Scale bar: 10µm. **F -** Quantification of complemented Venus fluorescence intensity at the membrane (co-localized with pmRFP) expressed as a percentage of whole cell Venus-fluorescence. Box and Whiskers plots of 21 to 54 measurements. *p<0.05, ***p<0.001, ****p<0.0001, Kruskal-Wallis test.

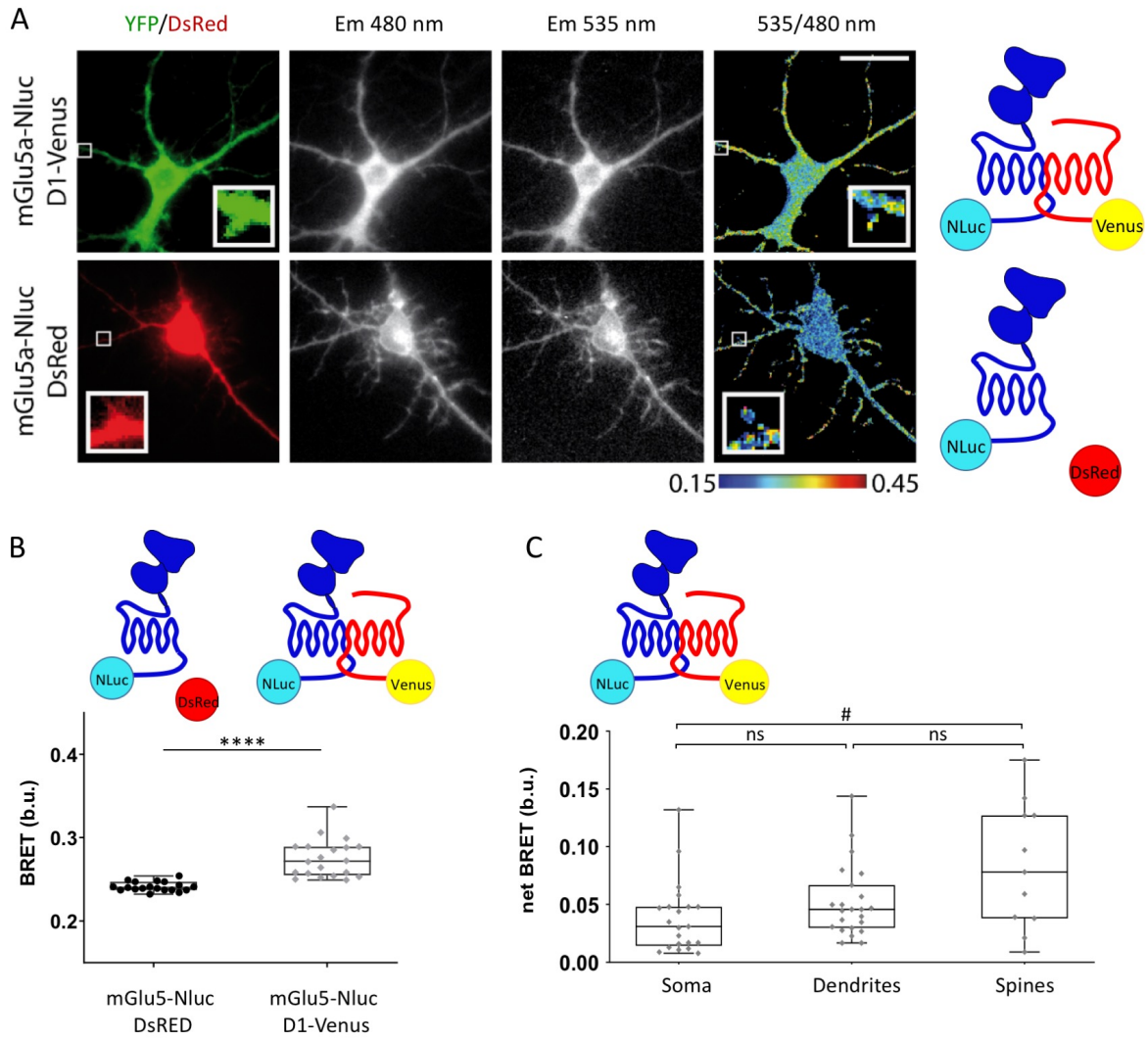

Figure 2 – D1 and mGlu5 receptors form heteromers in neurons

A-C – BRET imaging between mGlu5-Nluc and D1-Venus was measured in soma, dendrites and spines of hippocampal neurons. **A -** Single-cell BRET imaging in neurons expressing either mGlu5-Nluc and D1-Venus (top) or mGlu5-Nluc with DsRed as transfection reporter (bottom). Cells were identified by green or red fluorescence (left). Em480 and Em535 images were recorded and the 535 nm/480 nm pseudo-colored ratio images were processed. Square areas are shown at a higher magnification in the insets. Cells are representative of 19 to 21 cells. Scale bar: 10 µm. **B -** Quantification of the BRET signal intensity in soma from mGlu5-NLuc and D1-Venus transfected neurons, compared to the basal BRET measured in neurons expressing mGlu5-Nluc alone (left). Box and Whiskers plots of 19 to 20 measurements in the soma of neurons. ****p<0.0001, Mann-Whitney test. **C -** netBRET between mGlu5-Nluc and D1-Venus in soma, dendrites and spines. The average basal BRET in respective compartment has been subtracted from BRET measurements. Box and Whiskers plots of n=23 measurements in soma, n=21 in dendrites n= 11 in spines from neurons expressing mGlu5-Nluc and D1-Venus. # p<0.05, Kruskal-Wallis test.

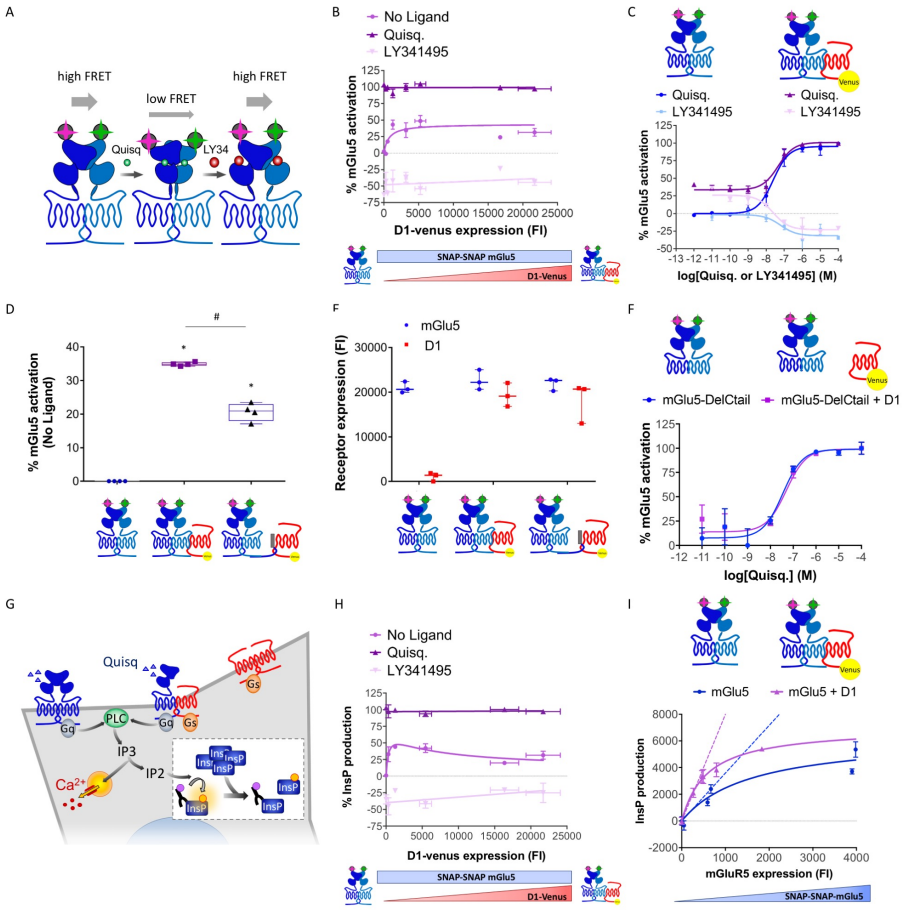

Figure 3 –D1-mGlu5 heteromer favors Ca^{2+} signaling *in vitro* by enhancing basal activation and basal signaling of mGlu5 receptor.

A – A TR-FRET based sensor monitors mGlu5 receptor ECD conformation. In absence of ligand or in presence of antagonist (LY341495), the proximity of TR-FRET donor and acceptor results in a high FRET signal. Agonist (Quisq)-induced relative movement of the extracellular ligand-binding domains decreases the FRET signal (28). **B-C -** Percentage of mGlu5 active-conformation measured with TR-FRET sensor **(B)** with increasing amount of transfected D1-Venus receptors in basal conditions (No Ligand), with Quisq (10µM) or with LY341495 (100µM) (FI: Fluorescence intensity); **(C)** in absence (blue) or presence (purple) of D1 receptor (corresponding to 279 ± 68 D1 FI on B) with increasing concentrations of Quisq (dark color) or LY341495 (light color). **D –** mGlu5 basal activation when expressed alone (left), with D1 receptor (middle), or with D1 receptor and mGlu5Ctail as dominant negative peptide for D1-mGlu5 interaction (right). *p<0.05 vs. mGlu5 basal activation, #p<0.05 vs. mGlu5 plus D1 receptor activation, Unpaired t-test (Mann and Withney). **E –** SNAP-mGlu5 and D1-Venus receptor expression levels were controlled by Fluorescence Intensity (FI) measurement of SNAP-Lumi4-Tb and Venus, respectively. **F –** Percentage of mGlu5-DelCtail active-conformation measured with TR-FRET sensor in absence (blue) or presence (purple) of D1 receptor with increasing concentrations of Quisq.

G – PLC activation is reported by new InsP production-induced decrease of HTRF signal between fluorescent-InsP and InsP-antibody (insert). **H -** mGlu5-induced InsP production with increasing amount of transfected D1 receptors in basal conditions (No Ligand), with Quisq (10µM) or with LY341495 (100µM). InsP production was normalized to the maximal activity of mGlu5 in presence of agonist. **I -** Constitutive InsP production with increasing amount of mGlu5 receptor in absence (blue) or presence (purple) of a constant amount of D1 receptor (corresponding to 319 ± 4 D1 fluorescence intensity on H). Values are mean ± SEM of 3 independent experiments.

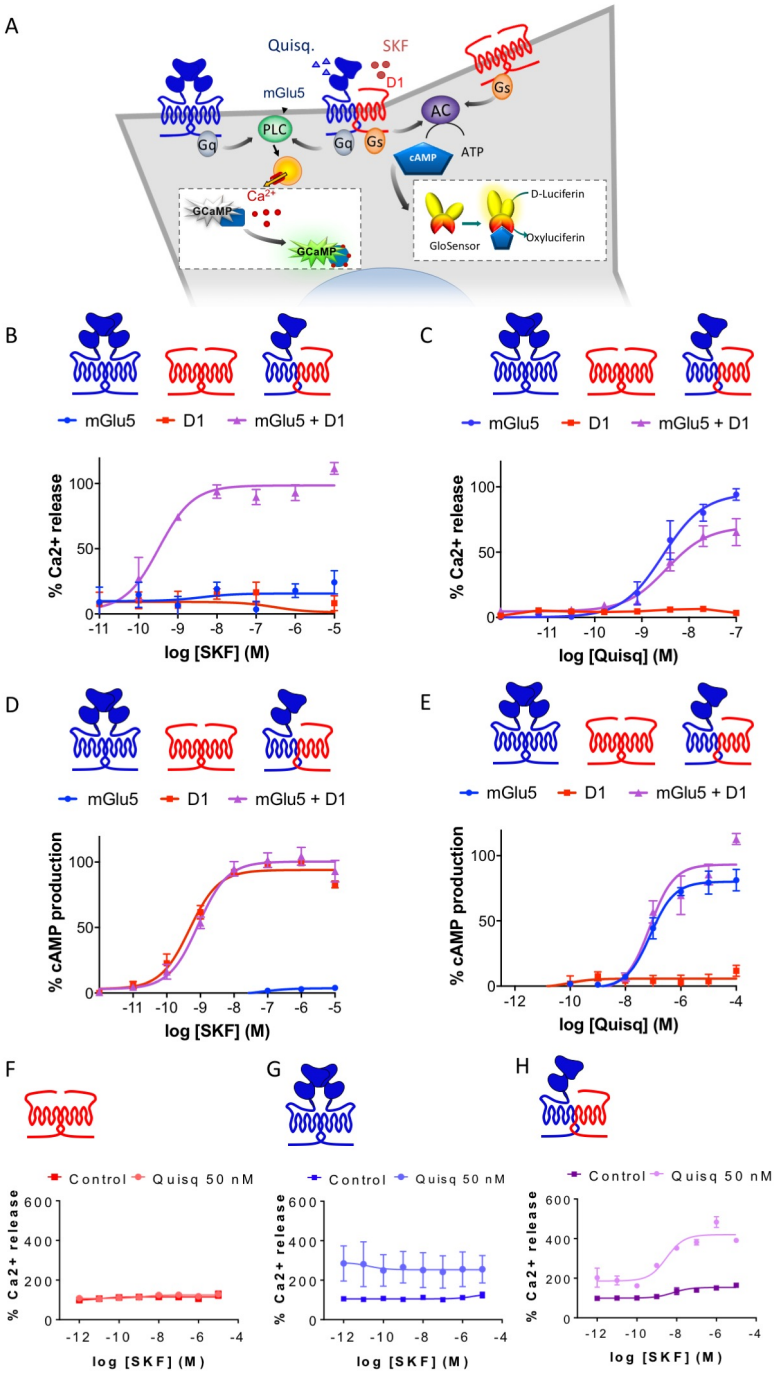

Figure 4 – mGlu5 receptor creates an atypical D1 receptor-mediated intracellular Ca^{2+} release.
A - HEK cell line stably expressing GcAMP6 calcium indicator and Glo cAMP-sensor, co-transfected with mGlu5 and D1 receptors. **B-E -** Ca^{2+} release and cAMP production were measured in cells transfected with mGlu5, D1 or mGlu5 plus D1 receptors. Values represent mean ± SEM of 3 or 4 independent experiments. Data are expressed as a percentage of the maximal Quisq- or SKF-induced effect. **B, C –** Ca^{2+} release dose-response curve induced by **(B)** D1 agonist (SKF81297) and **(C)** mGlu5 agonist Quisq. **D, E -** cAMP production dose response curve induced by **(D)** D1 agonist SKF81297 and **(E)** mGlu5 agonist Quisq. **F-H -** Synergistic activation of Ca^{2+} release induced by D1 and mGlu5 receptors. Cells were transfected with D1 **(F)**, mGlu5 **(G)** or both receptors **(H)**. Ca^{2+} release is here expressed as a percentage of basal levels in each transfection condition. Values represent mean ± SEM of 2-4 independent experiments.

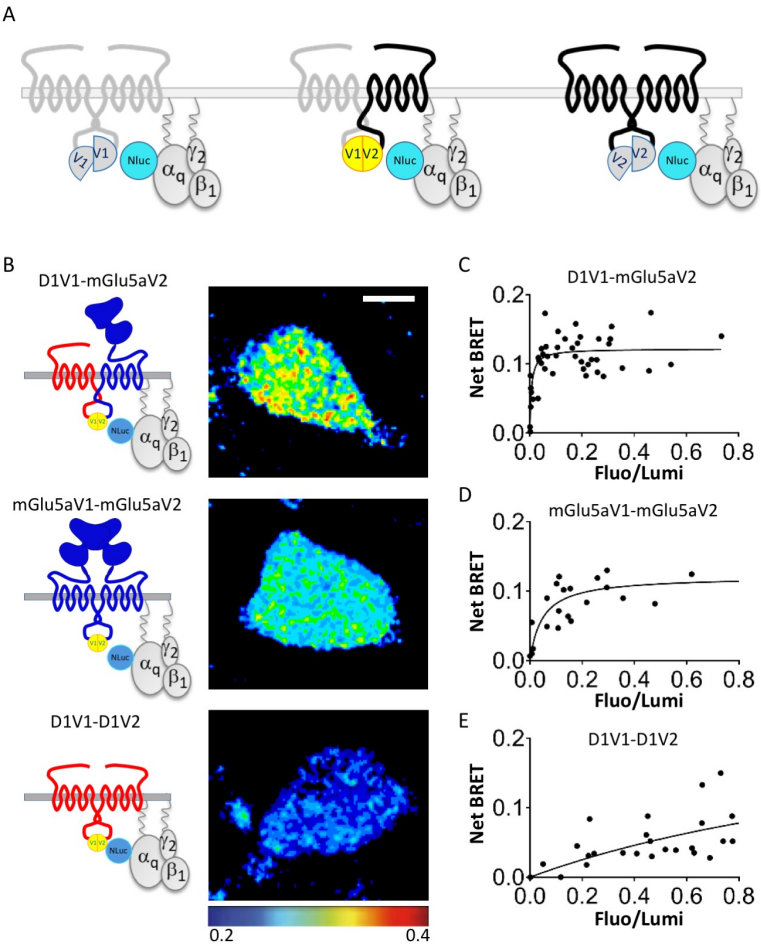

Figure 5 – D1-mGlu5 heteromer is coupled to Gq protein.

A - Complemented donor-acceptor resonance energy transfer (CODA-RET) enables exclusive monitoring of one dimer species of interest. **B-E -** CODA-RET imaging monitored on HEK cells expressing the indicated complemented dimers. **(B)** The pseudocolor images quantify the BRET between the complemented Venus-dimer and Nluc-Gαq protein. **(C-E)** BRET titration curves were measured for increasing acceptor/donor ratio (Fluo/Lumi). Results were analyzed by nonlinear regression on a pooled data set from three independent experiments, assuming a model with one-site binding (GraphPad Prism 7).

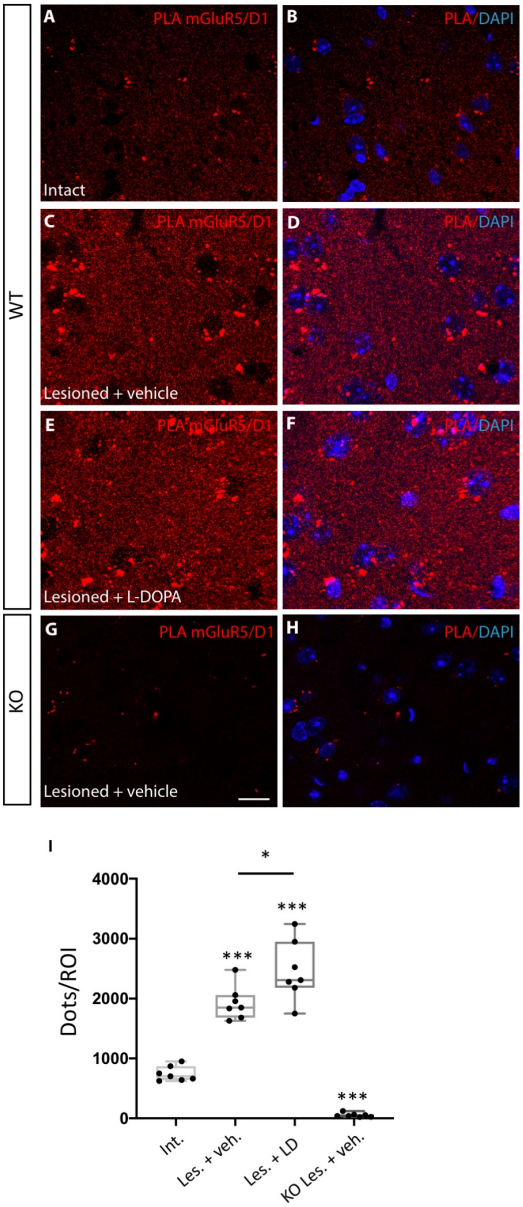

Figure 6 – Endogenous D1-mGlu5 clusters number is increased in DA-denervated striata

Protein Ligation Assays (PLA) experiments were performed on intact (**A-B**) and DA-denervated (**C-H**, Lesioned) striata of wild type mice (**A-F**, WT, n=7 per treatment condition) and mice with a selective knockout of mGluR5 in D1 receptor-expressing neurons (*mGlu5*$^{KO\text{-}D1}$; n=7) (**G-H**, KO). DA-denervated mice received daily s.c. injection of either L-DOPA (6 mg/kg) (**E-F**) or vehicle (saline, **C-D**, **G-H**) for 3 weeks. All L-DOPA-treated mice developed dyskinesia. **A-H -** PLA were obtained with primary antibodies directed against mGlu5 and D1. Plus and minus probes that correspond to secondary antibodies allow rolling-circle amplification and detection of the amplicons by a fluorescence labeled probe (red dots). Nuclei were counterstained with DAPI (scale bar: 10 μm). **I -** Graphs show the average of the number of PLA signals (reds dots) per pre-sized zone from Wt and KO striatal sections in indicated conditions. Error bars represent the SD. Six Regions of Interest (ROI) were analyzed per striatum to measure a mean value per animal. * $p<0.05$; ***$p<0.001$, Mann-Whitney test.

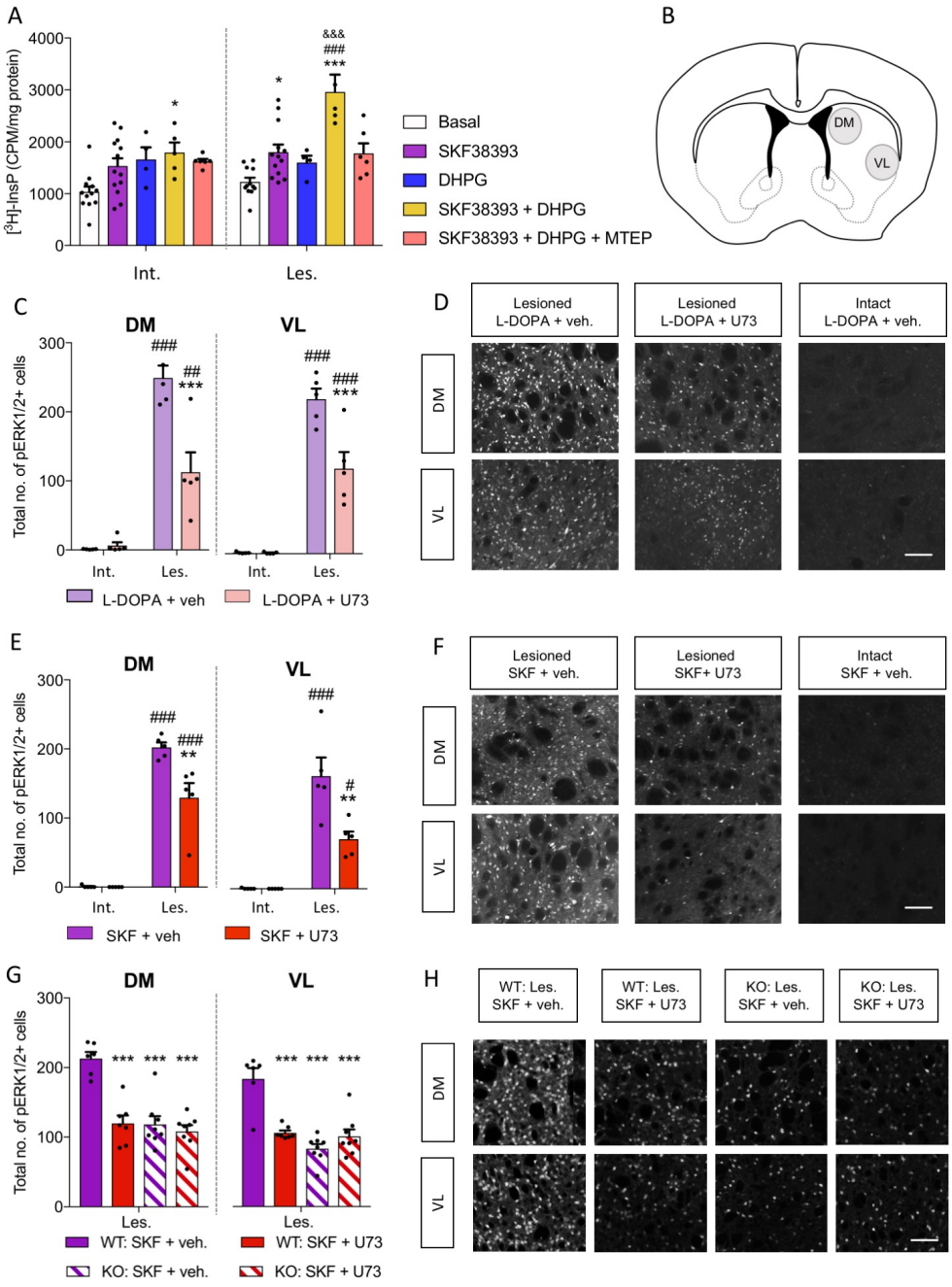

Figure 7 – mGlu5 and D1 receptors functionally interact to induce both PLC activity and ERK1/2 activation in the DA-depleted striatum.

(A) PLC activity was estimated using an assay of InsP hydrolysis in intact (Int.) and lesioned (Les.) rat striatal slices. SKF38393 and DHPG synergistically activated PLC in the DA-denervated striatum (n=4-13 per treatment. Treatment: $F(4,70)=14.33$, $p < 0.001$; Side: $F(1,70)=9.40$, $p < 0.01$; Interaction: $F(4,70)=2.81$, $p < 0.05$. Bonferroni's test: *$p < 0.05$ and ***$p < 0.001$ vs. baseline of same group; ### $p < 0.001$ vs. all other treatments within the same group (Les.) and &&& $p < 0.001$ vs. same treatment of opposite group (Int.). **(B)** Sample areas used for counting pERK1/2-positive cells in dorsomedial (DM) and ventrolateral (VL) striata from both rat and mouse. **(C-F)** U73122 (U73) attenuates the activation of ERK1/2 by L-DOPA (C-D) and SKF38393 (E-F) in the DA-denervated rat striatum (n=5 per condition). **(D,F)** Rat striatal

sections immunostained for pERK1/2, scale bar: 200 µm [C-DM: Treatment: $F(1,16)= 14.64$, $p < 0.01$; Side: $F(1,16)= 106.6$, $p < 0.001$; Interaction: $F(1,16)= 17.13$, $p < 0.001$. C-VL: Treatment: $F(1,16)= 12.57$, $p < 0.01$; Side: $F(1.16)= 146.1$, $p < 0.001$; Interaction: $F(1,16)= 12.36$, $p < 0.01$. E-DM: Treatment: $F(1,16)= 10.67$, $p < 0.01$; Side: $F(1,16)= 212.7$, $p < 0.001$; Interaction: $F(1,16)= 10.21$, $p < 0.01$. E-VL: Treatment: $F(1,16)= 9.99$, $p < 0.01$; Side: $F(1,16)= 65.29$, $p < 0.001$; Interaction: $F(1,16)= 9.82$, $p < 0.01$). Post hoc Bonferroni's test: **p < 0.01 and ***p < 0.001 vs. L-DOPA/SKF38393 + vehicle of Les. side; #p < 0.05, ##p < 0.01 and ###p < 0.001 vs. L-DOPA/SKF38393 + vehicle/U73122 of Int. side]. **(G-H)** U73122 attenuates D1-dependent ERK1/2 activation in DA-denervated striata from wildtype mice, but is without effect in $mGlu5^{KO\text{-}D1}$ mice (KO) (n=6-8 mice per condition). pERK1/2 immunostainings are shown in H, scale bar: 200 µm. [G-DM: Treatment: $F(3,25)= 18.63$, $p < 0.001$). G-VL: Treatment: $F(3,25)= 20.36$, $p < 0.001$). Post-hoc Bonferroni's test: ***p < 0.001 vs. Wt: SKF38393 + vehicle.]

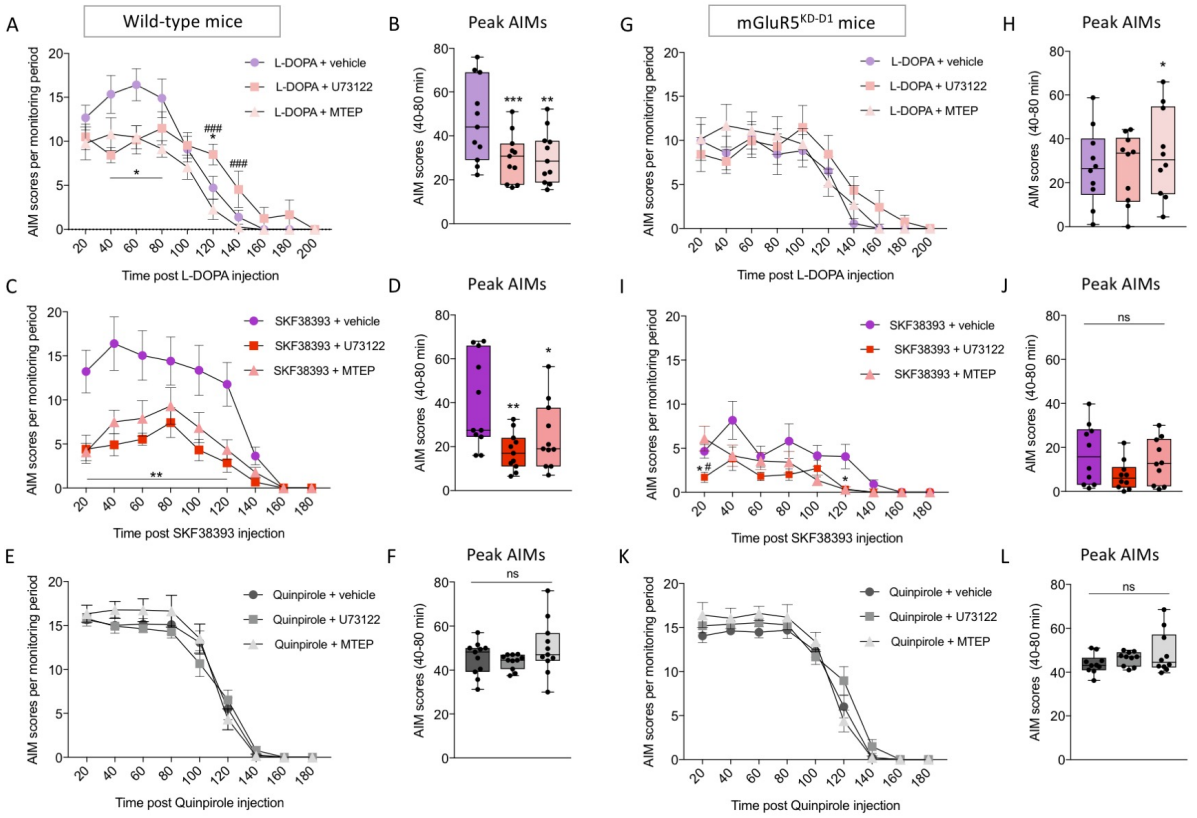

Figure 8 – MTEP and U73122 reduce dyskinesia in Wt mice but have no additional antidyskinetic effect in *mGluR5*$^{KD-D1}$ mice.

(A-B) L-DOPA-induced AIMs in wt mice. **A -** Time course of AIM scores in a test session (n = 11; RM Two-way ANOVA, Treatment: $F(2,20)= 13.6$, $p < 0.001$; Time: $F(9,90)= 45.87$, $p < 0.001$; Interaction: $F(18,180)= 4.49$, $p < 0.001$). **B -** Peak AIMs (n = 11; Friedman test (Fr) = 16.55, $p < 0.001$). **(C-D)** SKF38393-induced AIMs in wt mice. **C -** Time course of AIM scores (n = 11; RM Two-way ANOVA, Treatment: $F(2,20)= 17.28$, $p < 0.001$; Time: $F(8,80)= 23$, $p < 0.001$; Interaction: $F(16,160)= 5.05$, $p < 0.001$). **D -** Peak AIMs (n = 11; Fr = 11.45, $p < 0.01$). (**E-F**) Quinpirole-induced AIMs in wt mice **E -** Time course of AIM scores (n = 11; RM Two-way ANOVA, Treatment: $F(2,20)= 1.48$, $p = 0.25$; Time: $F(8,80)= 148.6$, $p < 0.001$; Interaction: $F(16,160)= 2.16$, $p < 0.01$). **F -** Peak AIMs (n = 11; Fr = 4.97, $p > 0.05$). (**G-H)** L-DOPA-induced AIMs in *mGluR5*$^{KD-D1}$ mice. **G -** Time course of AIM scores (n = 10; RM Two-way ANOVA, Treatment: $F(2,18)= 3.92$, $p = 0.31$; Time: $F(9,81)= 20.56$, $p < 0.001$; Interaction: $F(18,162)= 2.04$, $p < 0.05$). **H -** Peak AIMs (n = 10; Fr = 7.4, $p < 0.05$). (**I-J**) SKF38393-induced AIMs in *mGluR5*$^{KD-D1}$ mice. **I -** Time course of AIM scores (n = 10; RM Two-way ANOVA, Treatment: $F(2,18)= 5.42$, $p < 0.05$; Time: $F(8,72) = 17.33$, $p < 0.001$; Interaction: $F(16,144)= 3.23$, $p < 0.001$). **J - P**eak AIMs (n = 10; Fr = 5, $p > 0.05$). (**K-L)** Quinpirole-induced AIMs in mGluR5^{KD-D1} mice. **K**- Time course of AIM scores (n = 10; RM Two-way ANOVA, Treatment: $F(2,18)= 2.51$, $p = 0.12$; Time: $F(8,72)= 178.8$, $p < 0.001$; Interaction: $F(16,144)= 2.98$, $p < 0.001$). **L** - Peak AIMs (n = 10; Fr = 1.4, $p > 0.05$). Bonferroni's test or Dunn's test (for peak AIMs): *$p < 0.05$, **$p < 0.01$ and ***$p < 0.001$ vs. DA receptor agonist + vehicle; #$p < 0.05$ and ###$p < 0.001$ vs. DA receptor agonist + MTEP.